Finite Element Simulation of Orthogonal Metal Cutting using LS Dyna

by

Vishnu Vardhan Chandrasekaran

A thesis submitted to the Graduate Faculty of
Auburn University
in partial fulfillment of the
requirements for the Degree of
Master of Science

Auburn, Alabama
August 06, 2011

Keywords: Orthogonal Metal Cutting, Finite element analysis,
Simulation, LS Dyna.

Approved by

Lewis N Payton, Chair, Associate Research Professor of Mechanical Engineering
J T Black, Professor Emeritus of Industrial and Systems Engineering
Robert L Jackson, Associate Professor of Mechanical Engineering

Abstract

The current study focuses on building a 2-Dimensional finite element model to simulate the orthogonal machining process under a dry machining environment in a commercially available FEA solver LS Dyna. One of the key objectives of this thesis is to document the use of LS Dyna to model metal cutting, allowing other researchers to more quickly build on this work.

The work material used in this study is Aluminum 6061-T6 alloy. The tool material is tool steel, which is modeled as a rigid body. A Plastic Kinematic Material Hardening model is used to define the work material and the chip formation is based on the effective failure plastic strain. A constant coefficient of friction between the tool and work piece is used, the values for which are obtained from the experimental results. The simulation is carried out with a constant velocity with different rake angles and depth cuts. The cutting force and thrust force values obtained for each combination of rake angle and cut depth are validated against the experimental data obtained earlier at Auburn University.

The comparison of results shows that the cutting force predicted by the model is within 20 % of the actual experimental values. The thrust force is one third of the experimental value. The trends of both the cutting force and thrust force were in good agreement with the experimental results when plotted against either rake angle or depth cut, although the magnitude is not exact.

Including the effects of the tool in the cutting process by not modeling it as a rigid body may help in reducing the error value and by implementing the actual friction taking place should give us the exact results as that of real time experiments. This model could then be used to study the effects of forces and stresses while varying other cutting parameters, tool geometry, different tool-work material combinations and cutting environments. The model is considered valid enough to use for sensitivity analysis of the metal cutting process in aluminum alloy 6061-T6 which will be the subject of future research at Auburn University.

Acknowledgments

In the first place, I would like to thank my mentor and my advisor Dr. Lewis Payton, for rendering tremendous support, not only in this project but throughout my course, academically and morally, without whom, completion of my course work and the project would not have been possible.

I would also like to thank my committee members, Dr. J T. Black and Dr. Robert Jackson for their guidance and in this project.

A very special thanks to Yang Xu, graduate student in mechanical engineering department of Auburn University, who helped me learn the LS Dyna software and solve issues. I would also like to thank my colleauges, Dr. Sakthivel Kandaswamy, Prajwal Swamy Sripathi, Michael Friedman, and Justin Evans for their support and guidance with my work. Thanks to James Clark and Shanon Price from the network services at Auburn University for helping me set up and access the software and supercomputers.

I would take this opportunity to show my gratitude to my parents for rendering a constant support, encouraging and inspiring me throughout my life. A special thanks to all my relatives and friends far and near for motivating me to achieve more.

Table of Contents

List of Tables

List of Figures

List of Abbreviations

F_c Cutting Force; Force component acting in direction of motion of tool.

F_t Thrust Force; Force component acting in direction normal to shear plane.

F Frictional Force upon Chip

R Resultant Force

N Normal Force upon Chip

γ Shear Strain

k Shear flow stress of weaker material

Ar Real area of Contact

Aa Apparent area of Contact

n Strain Hardening Coefficient

T Temperature

$\bar{\sigma}$ Yield stress

$\bar{\varepsilon}^{pl}$ Equivalent plastic strain

μ Friction Coefficient

F_s Shear Force on the Plane

F_n Normal Force on the Plane

t Uncut Chip Thickness (also referred to as Feed Rate)

t_c Cut Chip Thickness

t/t_c Chip Thickness Ratio

A_s Area of the Shear Plane

τ_s Shear Stress on the Shear Plane

α Rake Angle

β Friction Angle

φ Shear Plane Angle

ψ Shear Front Angle

V Cutting Velocity

Vc Chip Velocity

Vs Shear Velocity

Introduction

The metal cutting industry utilizes different processes like milling, turning, shaping etc., to remove the material to form the required product. In all the fore mentioned process, material is removed in the form of chips by a single point or an oblique surface of the tool contacting the work piece at a relative force and this is termed as oblique cutting. Figure 1 depicts a typical oblique machining, such a process involves a 3 dimensional force system acting at the point of cutting which makes it complex for analysis and research work.

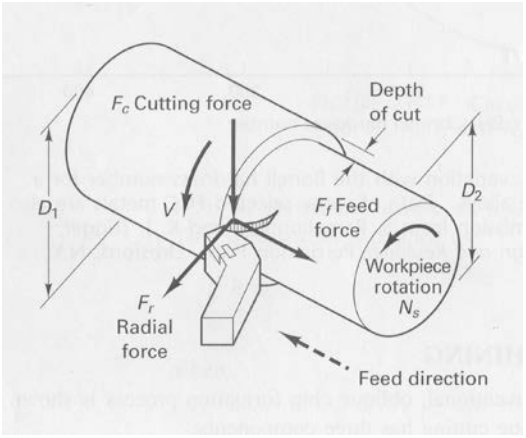

Figure1: A typical Oblique Machining Process [79].

There are a lot of major contributions made towards metal cutting industry in the past century of which a couple of them need s a special mention. The first one is the lecture delivered by F. W Taylor (1907) on “The art of cutting metals” in which up to twelve cutting variables that influenced the cutting speed selection were analyzed with a primary objective of “getting better and cheaper work out of machine shop” which was well supported by his yet another notable contribution Taylor equation to predict the tool life [1]. Piispanen and Dr. Merchant (1944) both independently put forth the concept of orthogonal cutting process concept where only two axis are considered at a given point of time which simplifies the complex 3 dimensional oblique cutting into a simple 2 dimensional orthogonal cutting process as shown in figure 2.

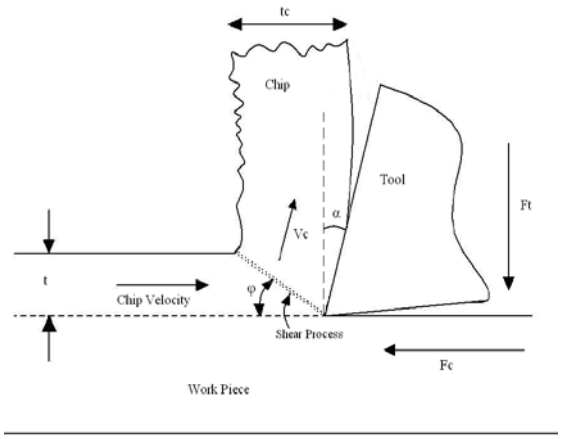

Figure 2: Orthogonal Machining

The concept of orthogonal cutting process is usually used for research process to study the effects of several parameters like velocity of cut, uncut chip thickness, tool geometries like rake angle, nose radius, clearance angle etc., on the forces involved in the

cutting process as well the wear on tool and the surface finish of the machined work piece.

Komanduri. R and Raff L M., 2001 [2] in his work states that nearly US $300 billion per year is spent in conducting metal cutting research in United States alone. This cost includes only the labor and over heads and does account for the raw material, cutting tools or machine tools. Another interesting fact mentioned by Komanduri is that for the experiments conducted by Taylor his team has utilized 363636 Kg of work material in the form of cast iron and steel over a span of 26 years in which they conducted nearly 30000 – 50000 experiments. The fact that conducting metal cutting experiments involves a huge investment is evident; there rises a need for alternative techniques to perform analysis to optimize the metal cutting process.

Demonstration to use concepts involving the finite elements modeling and analysis (FEA) along with growth in the field of computer technology has to an extent reduced the need for conducting the metal cutting experiments. A lot of researchers have applied the FEA concept to model metal cutting simulations, not many have validated the simulated results against the real time experiments to make the model more dependable/reliable. There are several commercial FEA simulation softwares available in the market ABAQUS, LS-Dyna, AdvantEdge to mention a few with each of them having its own advantages and disadvantages.

The current study focuses on building a 2-Dimensional Finite element model to simulate the orthogonal machining process under a dry machining environment in a commercially available FEA solver LS Dyna. A set of 20 simulations will be carried out

under different combinations of uncut chip thickness and tool rake angle. For this study 4 different tool rake angles and 5 different depths of cuts are considered on an aluminum 6061 T6 work piece and high speed steel tool. The cutting force and the thrust force obtained from the simulation will be validated against the results from real time experimental results [4] conducted at Auburn University.

Scope and Objectives

The goal of this thesis work is to develop a finite element model to simulate the orthogonal machining that could be used to study the effects of different cutting parameters, tool geometry, cutting environment and different work–tool material on the forces and stresses generated during metal cutting process. Such a model would serve as a platform for optimizing the metal cutting parameters to obtain better quality in machining, surface finish and to increase the life of machine tool.

The primary objective of this study is to develop a comprehensive finite element model to simulate and predict different forces and stresses involved in the Orthogonal machining process. It is intended to,

- Provide a thorough literature review on the existing simulation techniques for modeling machining problems.
- Construct a basic orthogonal machining model using LS Dyna FEA software.
- Vary the cutting conditions such as uncut chip thickness, tool rake angle and simulate the cutting process to study the variations in cutting force and thrust force and cut chip thickness.
- Validate the Cutting force and thrust force from the simulated data against the real time experimental results obtained from experiments conducted at Auburn University. Validate cut chip thickness versus actual chip thickness.

- Document the setup of LS Dyna for students using it to setup orthogonal machining simulations so as to reduce their steep software learning curve.

Literature Review

In the earliest reference, which could be found relating to scientific studies of the cutting process, Cocquilhat (1851) [24] centered his studies upon the cutting with a drill of a rotating work piece. From these fundamental studies, he was able to extend his basic observations of the metal cutting process to more worldly interests. With the knowledge of work required per unit volume of material removed and assumptions of wages and working days, he then made some calculations on the costs of digging tunnels, cutting marble and trench digging.

The first experiments in which the influence of tool geometry was studied were reported by Joessel (1865) [25]. Forces were obtained in lathe cutting and drilling by measuring the torque required to turn the machine while cutting, care being taken to subtract the torque required to overcome the friction of the machine. The effects of uncut chip thickness, speed and rake angle were studied. References to “cutting fluids” are also found in his work (linseed oil, quicklime and nitric acid to name a few), although no explanation of their benefit was attempted.

The first attempts to study chip formation are those of Time (1877) [26] and Tresca (1878) [27]. Time was the first to correctly model the process ahead of the tool as one of shear, although he may be criticized for his viewpoint that the chip formation took place by fracturing of the metal on successive shear planes rather than by plastic

deformation. This is understandable though since the plastic deformation of metals in operations other than cutting was only beginning to be investigated at the time.

Mallock (1881) [28] produced a set of drawings of polished and etched chips in 1881, which rival modern photomicrographs in quality. He deduced that the cutting process was one of shear along a sharply defined shear plane with friction occurring along the tool face. With Time, he thought of fracture as occurring on the successive shear planes and described the chip as a "metallic slate." Mallock observed that the friction between the chip and the tool decreased when a "cutting fluid" was applied. His drawings clearly show that when cutting copper, the use of soap and water as a cutting fluid increased the shear plane angle, which is most easily described as a line from the tip of the tool to the back of the undeformed chip, Figure 3. He was also the first to attempt to categorize the bluntness of the leading edge of the tool (the cutting edge) as a factor.

Haussner (1892) [29] was successful in building the first instrument, which could directly measure the forces involved in metal cutting. In this planning dynamometer, the work was restrained by a stiff spring. Deflections of the spring were magnified and a record was drawn by the dynamometer of the force against the distance of the cut. Although he was successful only in measuring the force horizontally along the cut, this was a major advance. He also noted the earliest comments on what appears to be the built-up-edge (BUE) in stating, "with ductile materials, after cutting starts, chips welded to the tool and were very hard to separate". He may also have been the first to deduce the presence of a normal stress along the shear plane, concluding that the elements were not "freely sheared but is under a normal pressure".

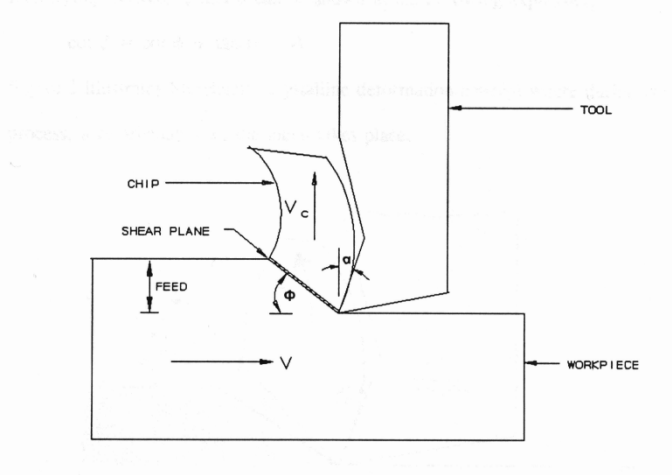

Figure 3: Shear Plane Angle and Tool Rake Angle

Zvorkin (1893) [30] published an extensive review of "planing" in 1893 using his new hydraulic dynamometer. He concurred with Haussner that the resultant force was not necessarily in the cutting direction. Assuming that the force in the direction of the cutting velocity would be a minimum led him to conclude the first attempt to predict the shear plane angle of Figure 3. in terms of the tool rake angle α and friction angle β

$$\phi = 45 + \alpha/2 - \beta/2 - \beta'/2 \tag{1}$$

where Φ corresponds to the shear plane angle, β is the friction angle on the chip and β' is a friction angle for the shear plane itself. This is the first of many formulations of the functional relationship amongst the various angles detailed shortly in an attempt to formulate a predictive relationship based upon the observed geometries at the tool interface. This equation will appear again in the literature review of modern theory, with β' equal to zero:

$$\phi = 45 + \alpha/2 - \beta/2 \tag{2}$$

Equation 2 was derived independently in 1896, in the German engineering handbook "Ingenieur und Maschininenmechanick" (1896) [31]. The basis of derivation in that case was that the shear plane would be the plane of maximum shear stress. The German handbook marks the beginning of the ongoing search for a predictive approach to the shear plane angle that eludes engineers to the current day. It carefully compared equations 1 and 2 at great length, offering reasons for the disagreement. Those equations continued in the literature after the turn of the 20th century. Lindner (1907) [32] followed by Ernst and Merchant [33] in 1941, obtained equation 1, while Piispanen (1937) [34], and Merchant (1945) [35], obtained equation 2. The development of the many versions of this predictive equation will be detailed at great length in the Shear Zone Section, since the nature of the material action within this zone will be one of the objectives of this experiment.

Force analysis would continue to improve to the current day dynamometers and began to be joined with photographic studies in the "Roaring Twenties" when Coker and Chakko (1925) [36] carried out experiments in 1924, and Coker (1925) [37] in 1925 carried out a series of photoelastic experiments on the action of cutting tools. They were able to show in their photographs that there were zones of approximately radial compression and tension ahead of and behind a line going forward from the tool point, which corresponds to the plane defined by the angle Φ in Figure 3. Coker's photographs were not taken during cutting however, but during a stoppage of the tool.

Ishi (1929) [38] and Schwerd (1935) [39] were the first to study the cutting process while cutting was actually in progress. Photographs were also taken through a microscope by Boston (1930) [40], which presented detailed appearance of the metal cutting process. Their photographs were instrumental in the thought processes of the metal cutting investigators of the 1940's and continue to be highly regarded today by photographic experts in the metal cutting field.

It was also at this time that one of the first experiments examining hardness was conducted in 1926 by Herbert (1926) [41]. He showed that the chip material was harder than the work material and demonstrated that metal cutting involved intense strain hardening which could only come about through the mechanisms of plastic deformation or flow.

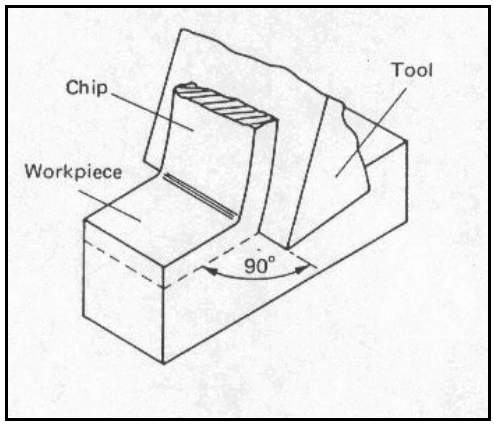

Figure 4: Orthogonal Machining Cut (Boothroyd et al, 1989) [42]

Orthogonal cutting such as depicted in Figure 4 is seldom used in practice, although it remains the simplest model for scientific analysis. Nearly all of the practical cutting processes are oblique, where the leading tool edge is inclined to the relative

velocity vector between the tool and work. Even in today's computer age, modeling such a difficult geometry remains a daunting task. Thus, it is necessary to consider how the mechanics of the orthogonal cutting can be extended and altered to describe oblique cutting.

Dr. Merchant's work in 1944 [1] presented a simplified 2-D model of the conventional oblique machining process called the orthogonal machining process which considers only two axes at a time which is also one of the widely used research model as it involves less complicated computations, easier to analyze and moreover is found to be in good agreement when extended to a 3-D model. Merchant's orthogonal machining model is of two types 1) orthogonal plate turning at moderate and high speeds (OPT), 2) orthogonal tube turning at moderate speeds (OTT) and is generally characterized by the following: [79]

- The cutting edge is sharp and there is no contact with the work piece on the clearance face.
- The plane of the cutting edge is perpendicular to the direction of motion.
- The tool moves at a constant velocity and uncut chip thickness generating the chip.
- The cutting edge on the tool is wider than the thickness of the work piece machined.

The work describes a geometrical model of the force system commonly referred to as Merchant's force diagram / merchant's circle is shown in figure 5. Fc is the cutting force acting along the horizontal axis at the tool tip and the work piece interface due to

the motion of the work piece against the tool which is also accompanied by the thrust force Ft acting in the vertical axis perpendicular to the Fc at the same instance.

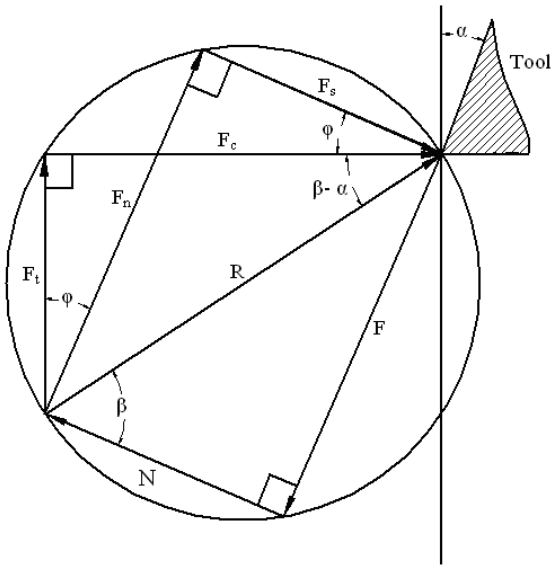

Figure 5: Merchant's force diagram [71].

There are three different chip types [67] mentioned in the literature as first documented by Ernst and they are: Type 1: Discontinuous or Segmented chip, Type 2: Continuous and Smooth chip and Type 3: Continuous chip with built up edge (BUE) of the chip material between the tool and chip.

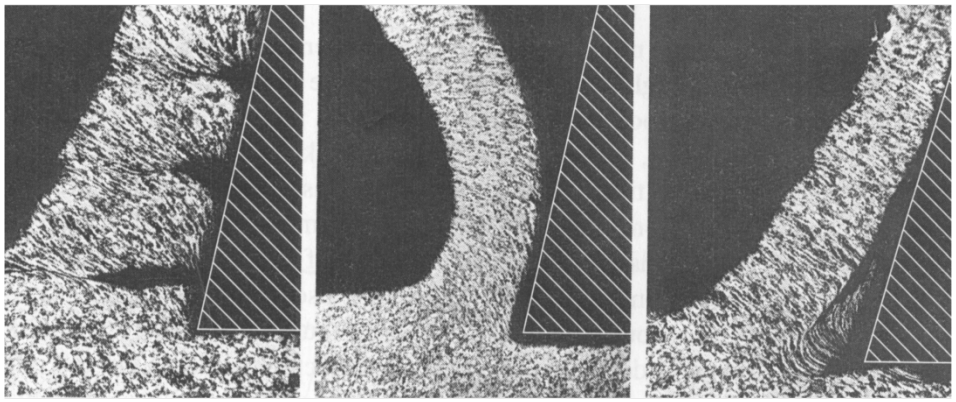

Figure 6: Type 1, 2 and 3 chips in that order.

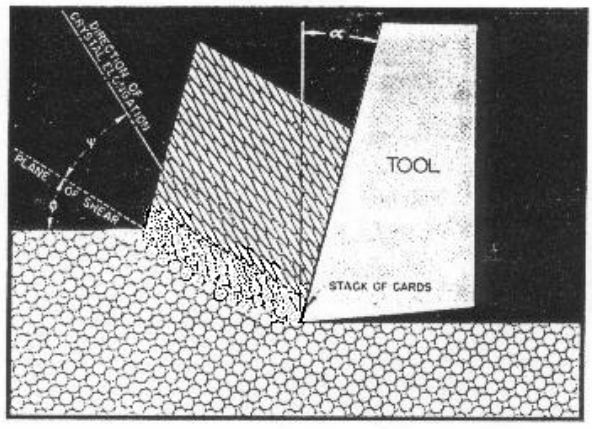

Figure 7: Merchant's observation of chip formation (Merchant, 1945) [1]

Merchant's model represented the shear zone as a single plane, or thin-zone model. The angle of inclination of the shear plane to the cutting direction was defined by the angle Φ. Merchant observed that the crystal structure of the material was elongated by the shear process and called direction of crystal elongation the direction ψ.

Merchant did not develop the plastic deformation aspect of his observations. Both Merchant and Piispanen used a "deck of cards" concept to visualize the shear zone process, where the shear mechanism during chip formation can be illustrated by the incremental displacement of cards in a stack (Figure 8). Each card moves forward a small amount in respect to the next card in the stack as the cutting process occurs. Merchant (1945) [1] proposed that the shear process elongated the crystalline structure of the metal, and that the direction of elongation was in a different direction than the shear plane.

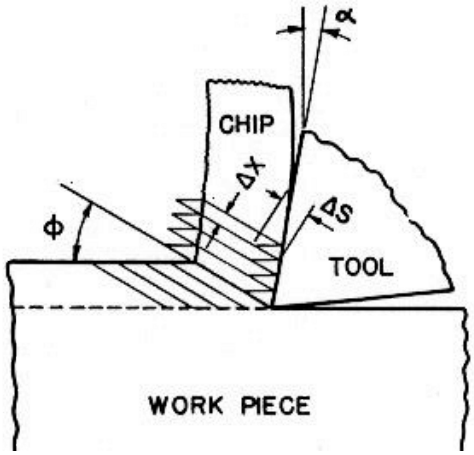

Figure 8: Merchant's Stack of Cards Model (Merchant, 1945) [1]

The thickness of each card element was ΔX, and each element in the model was displaced through distance ΔS with respect to its adjacent neighbor. Therefore, the shear strain, γ, could be expressed as $\gamma = \Delta S / \Delta X$. From the geometry of his stack of cards, Merchant thus developed the following equation:

$$\gamma = \frac{\cos\alpha}{\sin\phi \times \cos(\phi - \alpha)} \tag{3}$$

Ernst and Merchant would eventually observe (Ernst and Merchant, 1941) [33] that the angle between the resultant force R and the shear plane was thus given by:

$$\phi = 45 + \frac{\alpha}{2} - \frac{\beta}{2} \tag{4}$$

Equation 4 was the first of many modern attempts to derive a functional angle relationship f(α,β) of some type. It has come to be referred to as the Ernst and Merchant solution (Eggleston et al, 1959) [43]. Although independently derived, this is again the result Zvorkin published in 1893 [30].

Lee and Shaffer (1951) [44] examined the geometry by considering that a part of the chip would behave as an ideal plastic solid. Using Mohr diagrams they developed the following relationship amongst the angles of the Merchant model:

$$\phi = 45 + \alpha - \beta \tag{5}$$

Thus both equation 4 and 5 suggest a strong interaction between the frictional angle and the tool rake angle in determining the shear plane angle. This has not proven to be a very satisfactory observation. Eggleston et al (1959) [43] noted in his detailed review of the observations of the angle relationships that neither the Ernst nor Merchant formulation, based upon the minimum energy criterion, or the ideal plastic-solid solution of Lee and Shaffer, nor the mathematical derivations of Hill are in agreement with all the experimental observations.

Merchant's model has been extensively examined, published and cited as the first thin-zone model. It has been seriously criticized by some academics because of its inability to describe the actual deformation process in machining. For example, a particle moving along the cutting direction into the shear plane must abruptly change direction at the plane and then flow in the direction of the chip. This represents a discontinuity in the tangential component of velocity on the shear plane, requiring an infinite acceleration across the shear plane. An examination of the action at the edge of the deformation zone is one of the goals of this experiment and a further review of the many shear zone models is continued below.

Okushima and Hitomi (1961) [45] developed a simplified thick-zone model in 1961, which is depicted as Figure 9 They suggested a very large transitional zone AOB.

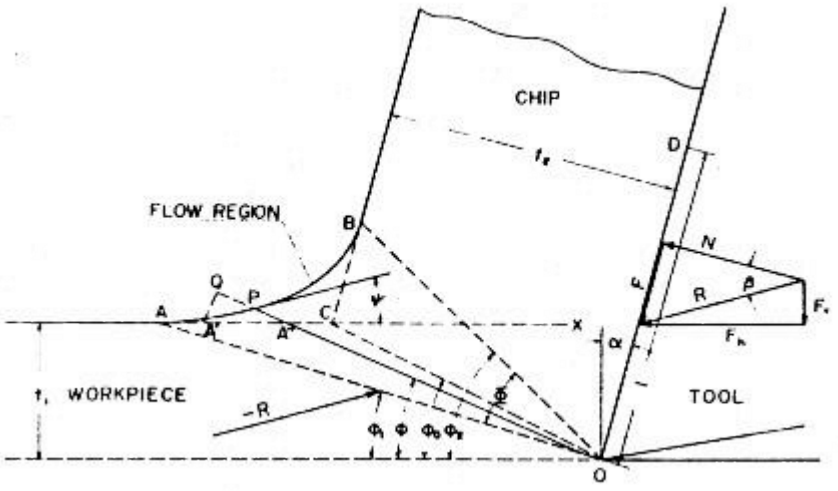

Figure 9: Okushima and Hitomi's Model (Okushima et al, 1961) [45]

The AOB zone existed for plastic deformation of metal between the rigid region of the workpiece and the plastic region of the steady chip as it moved away up the tool face. Plastic deformation began to occur at the starting boundary line of the shear zone, OA, and the plastic strain gradually increased as the cut progressed. Shear strain inside the shear zone AOB was expressed as follows:

$$\gamma = \cot\phi - \cot(\phi - \Psi) \tag{6}$$

Here Φ is the inclination angle of the arbitrary radial plane, and ψ is the tangent to the free surface (curve between A and B in Figure 9) with the machined surface. This model predicted that the shear strain was zero at the lower boundary of the shear zone and obtained the maximum at the upper boundary of the shear zone.

In 1966, Zorev (1966) [46] proposed the thick zone model detailed in Figure 10. Line OL defined the initial boundary of the zone and OM the final boundary of the shear zone. Inside the shear zone LOM, there was a family of shear lines along which shear

deformations were formed. Work material passed through the shear zone and was subjected to increasing shear strain:

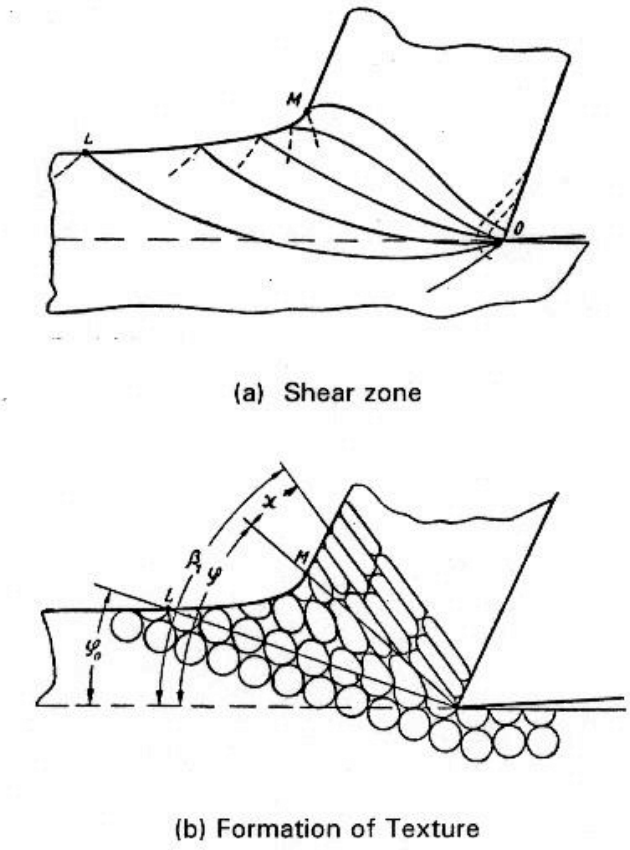

Figure 10: Zorev's model of a thick zone (1966) [46]

The initial boundary of shear zone is similar to the onset shear plane proposed by Black in a later paper [80]. The direction of shear deformation was tangent to each line. The shear direction was approximately parallel to the initial boundary of the shear zone.

Zorev's expression of the shear strain is the same as equation 6 above. The texture of the chip formation, due to shear deformation, changed from an equiaxial structure into a non-equiaxial structure. The angle ψ in his formulation, between the

direction of the texture and the direction of the plastic shear, was a function of the degree of plastic deformation and was determined by the following relationship:

$$\cot \Psi = \frac{\gamma}{2} + \sqrt[2]{1 + \frac{\gamma^2}{4}} \tag{7}$$

Oxley (1989) [18] proposed a parallel-sided shear zone model in 1989 as depicted in Figure 11. The total maximum shear strain in the shear zone was found by multiplying

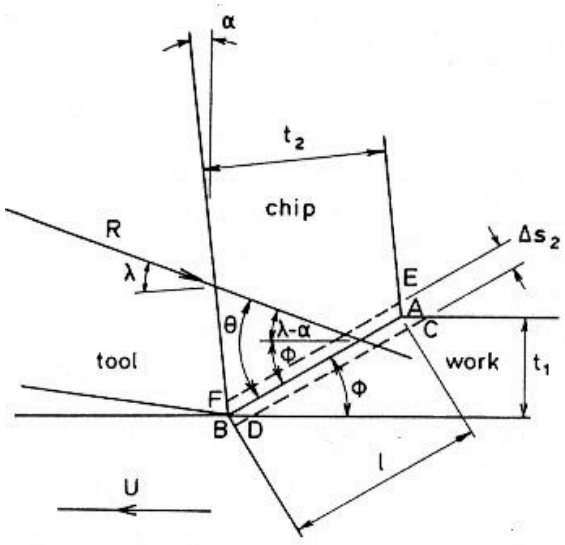

Figure 11: Oxley's Parallel-Sided Shear Zone Model (Oxley, 1989) [18]

the average maximum shear strain-rate in the zone by the time a particle took to flow through the zone. Maximum shear strain was expressed as

$$\gamma_{ef} = \frac{\cos \alpha}{\sin \phi \times \cos(\phi - \alpha)} \tag{8}$$

It was assumed that one half of the total strain in the shear zone occurred at the centerline, AB. The shear strain in the plane defined by AB was taken as

$$\gamma_{ab} = \frac{\cos\alpha}{2 \times \sin\phi \times \cos(\phi - \alpha)} \tag{9}$$

Oxley depicted the direction of elongation in his zone model as shown in Figure 12.

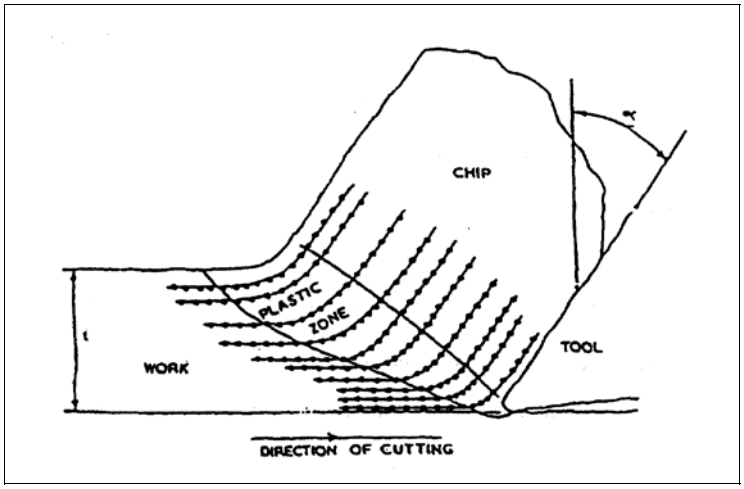

Figure 12: Oxley's Direction of Shear Zone Flow [18]

A "stationary" shear zone model was presented by Von Luttervelt (1977) [47] as depicted in Figure 13. This model is similar to Oxley's parallel-sided shear zone model.

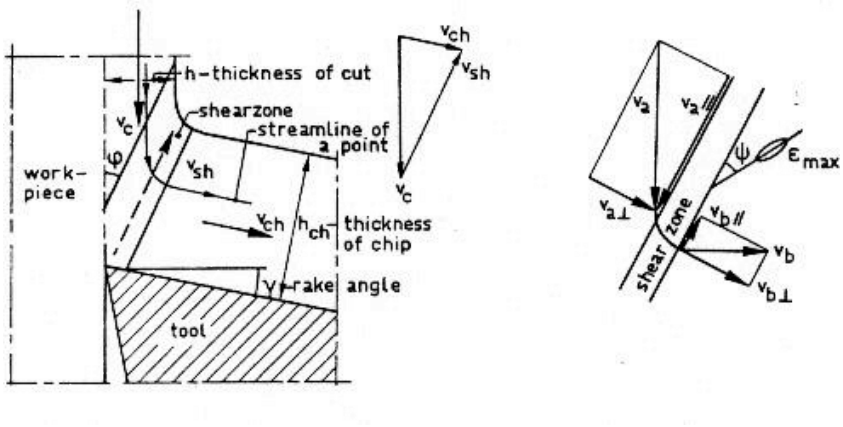

Figure 13: Van Luttervelt's Stationary Shear Zone Model (Von Luttervelt, 1977) [47]

The material entered the shear zone with velocity V_a, which might be resolved into two components, one parallel to the shear zone and the other perpendicular to the shear zone. The material left the zone with a velocity V_b, which could also be decomposed into its parallel and perpendicular components. The shear strain within the zone was derived from these components as:

$$\gamma = \frac{\cos(2\times\phi - \alpha)}{\sin\phi \times \cos(\phi - \alpha)} \tag{10}$$

The direction of maximum elongation described in Van Luttervelt's model is the same as in Oxley's model.

Another shear zone model was suggested in 1996 by Huang (1996) [50], working as a graduate student for J T. Black. During a review of Briggs' (1993) experiment using high-speed magnification to observe the cutting of aluminum, Huang developed a new "stack of cards" model and a new shear strain equation of orthogonal machining. In reviewing the tapes made by Briggs, they observed that the material deformed in a totally different fashion than that which had been described in the machining literature. The plastic deformation of material as observed by Huang and Black is depicted in Figure 14.

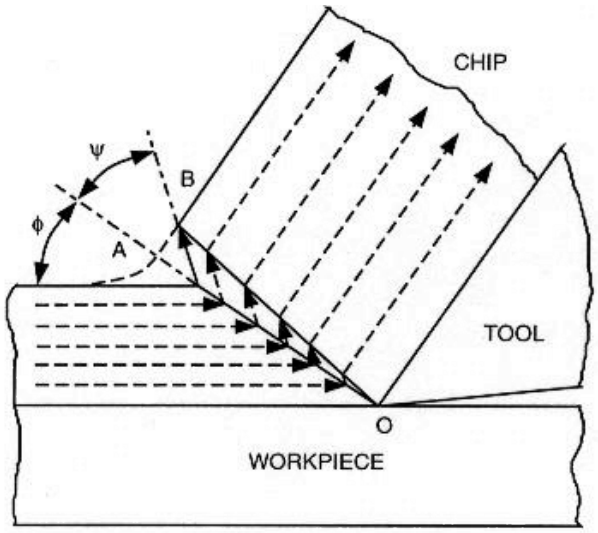

Figure 14: Huang's Observation of Flow in Shear Zone (Huang, 1996) [50]

Upon reaching the plane BO, the shearing process stops, and the material changes direction a final time and moves in a direction parallel to the tool face. The shape of AOB is triangular and the onset shear plane is flat. The material encounters plane AO simultaneously and shear is in mass all along the boundary. This onset of shear fronts creates the shear plane and defines the lower boundary of the shear zone. Thus Φ has been more properly termed by Black the Onset of Shear Plane angle (Black, 1979) [48]. The termination of the shear fronts forms the upper boundary of the shear zone as noted by Black and Briggs (Black et al, 1994) [49]. The shear fronts are inclined at an angle, ψ, originating from the plane connecting the tool tip to the free surface. His reasoning behind this movement was the presence of dislocations in the material. Figure 15 details the angular relationships as derived by Huang.

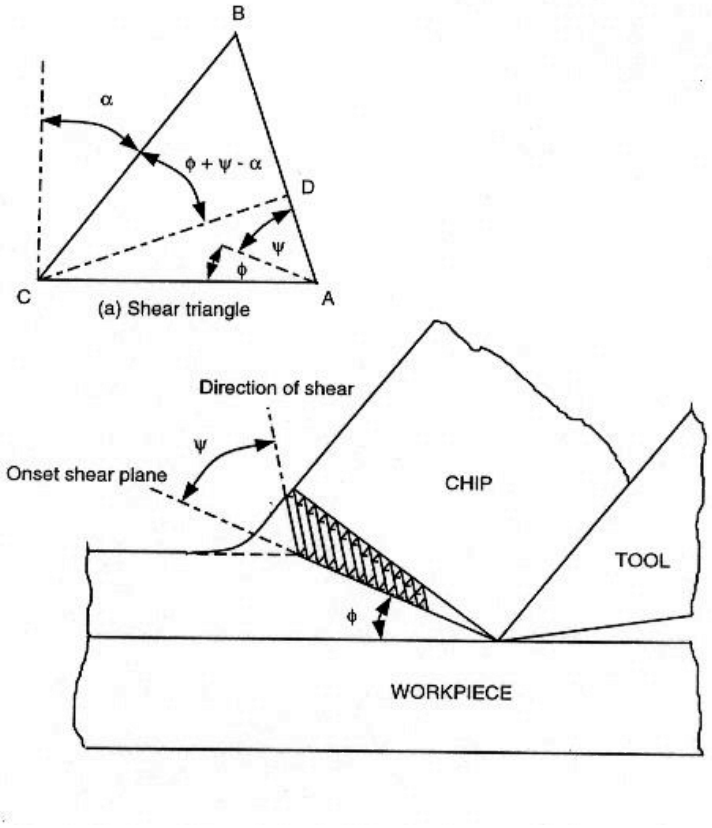

Figure 15: Huang's "New" Stack of Cards Model (Huang, 1996) [50]

Huang's model is significantly different than Merchant's model. In the new card model, an element shears at the direction ψ relative to the onset shear plane. (In Merchant's model, an element shears in the direction of the shear plane Φ. In Zorev's model the work material shears tangentially to a shear line that is approximately parallel to the initial shear plane.) Using a minimum energy criterion, Huang developed the following relationships for ψ and γ:

$$\varphi = 45 - \phi + \frac{\alpha}{2} \tag{11}$$

$$\gamma = \frac{2 \times \cos\alpha}{1 + \sin\alpha} \tag{12}$$

The general mechanism of deformation in orthogonal cutting involves shearing at the primary shear zone where the chip is formed and the formation of a secondary shear zone where the chip undergoes further shearing as it slides along the tool face accompanied by friction effects. The classical description of chip formation for most materials as cutting speed is increased within the conventional speed range (1-100 m/min) starts initially with a discontinuous chip (Type I), a continuous chip with a built-up edge (Type III) and finally a continuous chip (Type II). With further increases in speed, the chip formation process is affected by instabilities in the cutting process both at the primary and in the secondary shear zones, yielding chip segmentation. The sources of such instabilities have been a subject of great controversy and research (Komanduri et al, 1981, Lemair et al, 1972, Komanduri et al, 1982, Komanduri et al, 1982, Sullivan et al, 1978, Shaw, 1993) [51-55].

At very low cutting speeds (<1 in/min) the mechanism of formation of discontinuous chips has been reported by Cook et al (1954) [56]. When the cutting speed is increased beyond the conventional speed range instabilities in shear occur, resulting in the formation of partially segmented chips. According to Komanduri and Brown (1982) [52], segmented chips form due to instabilities of the workpiece both in the primary and secondary shear zones, and the dynamic response of the machine tool structure contributes to their formation. Instability in the primary shear zone has been attributed to the negative stress-strain characteristics of certain materials at large strains, involving void formation around second phase particles, their propagation into micro-cracks and coalescence of these cracks leading to partial fracture (i.e. geometrical instability). The

instability at the secondary shear zone is due to stick-slip friction of the chip segment on the tool-face.

Sullivan, Wright and Smith (1978) [54] attributed the formation of segmented chips to seizure and strain rate hardening of the material at the rake face. In the first part of the contact length near the tool tip, the material strength increases due to work hardening so that the primary shear zone becomes the weaker region in which shear takes place. Due to temperature softening near the end of the secondary shear zone, the material at this region has a lower strength allowing flow to take place thus establishing stick-slip friction at the secondary shear zone with an attendant variation of the shear plane angle. The process is repeated with formation of a new segment. The analysis provided by Sullivan et al (1978) therefore introduced the flow stress and the material's strain rate sensitivity as key factors on which chip segmentation depends, while discounting the primary shear zone as the source of large-scale heterogeneity. Shaw (1993)[55] has proposed that chip segmentation in 60/40 brass and hardened steel is caused by periodic gross fracture extending from the free surface of the chip toward the tool tip. There is insufficient quantitative experimental evidence in the literature to validate the mechanisms so far proposed.

Further increase in speed beyond the critical speed for adiabatic shear culminates in the formation of shear-localized chips due to catastrophic shear at the primary shear zone (Komanduri et al, 1981, Komanduri et al, 1982, Shaw, 1993, Recht, 1964 and Komanduri et al, 1986). Lemaire and Backofen (1972) [53] investigated possible adiabatic instability in orthogonal machining of tempered martensitic steel (Fe 18.5% Ni

0.52% C) by observing the reverse transformation of martensite into austenite in the primary shear zone. The discontinuous chips formed exhibit white-etching bands between the segments; hence they are of the type described by Komanduri et al (1984) to be shear-localized chips. The authors proposed the formation of this type of chips to involve localized deformation confined to a narrow zone extending from the tip of the tool to the free surface of the test strip. They used Loewan and Shaw's (1954) [57] thermal model for continuous chip formation to calculate the shear zone temperature, taking average values of shear strain calculated from the chip thickness measurements. The temperatures obtained were below 200°C, which are far below the transformation temperature of the material (426°C) and therefore insufficient to bring about the observed reversion of martensite to austenite. They suggested periodic release of the system stored elastic energy into the chip once the system becomes mechanically unstable as a potential energy source which raises the temperature in the adiabatic shear band beyond the transformation temperature of the material. This model based on experimental results at low cutting speeds where the frequency of chip segmentation is low and at or near the natural frequency of the system is a plausible explanation. However, the validity of the model under high cutting speeds where the frequency of oscillation is very high and far beyond the natural frequency of the system is doubtful. Due to inherent damping, the effect of overall machine tool response at those high frequencies of chip segmentation when machining at high cutting speeds should be minimal. The authors proposed three conditions upon which reversion of martensite to austenite depend:

(1) Deformation must be confined to a shear zone,

(2) Temperatures in the shear zone must reach the level at which the criterion for adiabatic instability is met,

(3) Rapid shearing during instability must raise the temperature further beyond the transformation temperature.

The influence of pressure on phase transformation and the influence of phase transformation on adiabatic shear localization was not addressed. It is not clear from Lemaire and Sakofen's results whether phase transformation causes adiabatic shear localization or is incidental.

The shear-localized chip has been observed with difficult-to-machine materials such as AISI 4340 steel (Komanduri et al, 1982) [52], Ti-6AI-4V (Komanduri et al, 1981) [51] and Inconel 718 (Komanduri et al, 1986) [58]. The formation of shear-localized chips may be caused by either (a) concentration of thermal energy in narrow bands because of poor thermo-physical properties of the workpiece material, or (b) concentration of thermal energy in narrow shear bands due to insufficient time for dissipation of heat from these bands at the high strain rates encountered at high cutting speeds (Komanduri et al, 1982). Two different mechanisms have been proposed to describe the formation of fully segmented chips at high cutting speeds. The first mechanism by Komanduri and et al (1984) [59] proposes that the formation of fully segmented chips, which they referred to as shear-localized chips, begins with plastic instability, leading to strain localization along a shear surface originating from the tool tip almost parallel to the cutting velocity vector and gradually curving until it meets the free surface. The formation of the chip is completed by gradual upsetting of the inclined wedge of the material ahead of the advancing tool. There is almost no relative motion

between the bottom surface of the chip segment being formed and the tool face almost until the end of the flattening stage. Therefore rapid transfer of heat occurs at the tool tip. There is periodic development of concentrated shear band of very large strain accompanied by rapid shear, i.e. adiabatic conditions prevail at the primary shear zone. An interesting feature of this model is that it proposes little or no secondary deformation along the rake face. Instead it proposes that the chip rolls over the tool face during the flattening stage. This implies that the formation of fully segmented chips does not involve seizure. If this is true then dissolution wear should be minimized at the tool-chip interface. The second mechanism by Shaw (1993) [55] proposed that adiabatic shear is not the root cause of chip segmentation at high cutting speeds. Instead Shaw proposed that chip segmentation at high cutting speeds occurs by periodic gross fracture extending from the free surface of the chip toward the tool tip. Thus the mechanism of formation of fully segmented chips at high cutting speeds and the influence of interfacial conditions on the mechanism does not appear to be resolved. New models should attempt to postulate the mechanisms of formation of segmented and shear-localized chips, and the resulting effect on tool wear mechanisms, based upon the properties of the material being cut.

In metal cutting the type of friction occurring at the tool-chip interface is mainly solid friction. Solid friction can be defined as the resistance to movement of one solid body over another. In metal cutting the movement may involve sliding or seizure at the tool-chip interface.

Traditionally, it has been assumed that coulombic friction controls the interface forces at low loads and that as the load grows to the point where the real area of contact is

equal to the apparent area of contact, friction becomes independent of pressure and takes on the value of *k*, which is the shear flow stress of the weaker material (Bowden et al, 1964). In metal cutting, *k* is not a simple value. It is modified by the hydrostatic pressure, high strain rates, large strains and high temperatures at high cutting speeds so that the final value is lower than the *k* determined from uniaxial tension tests (Ling et al, 1987) [60]. A recent analysis of friction in metal working processes based on slip line field studies has been presented by Kopalinsky et al (1991) [61]. The frictional processes in metal cutting are complex because of the existence of very high normal loads. Friction under high normal loads has been discussed in detail by Thomsen (1969) [62]. An increase in the normal load across the contacting surfaces produces an increase in the real area of contact. Relative motion between the surfaces produces shearing of welded asperities and some subsurface plastic flow.

The frictional force F is given by the equation $F=A_rS$ where S is the shear strength of the asperities of the softer material, but is not linearly related to the normal force N. In Region II of Figure 16, it has been shown that at very high normal loads the real area of contact approaches the apparent area of contact A_a. With this condition A_r has reached its maximum value ($A_r/A_a=1$) and conditions of sticking friction are said to exist. Relative motion between the surfaces produces gross subsurface flow and the coefficient of friction reaches its limiting value of 0.577 if it is assumed that the Von Mises flow rule applies. Then the frictional force F is independent of the normal force N and the coefficient of friction decreases with a further increase in normal load. Friction in metal cutting occurs at the flank and the rake faces of the tool. There is ample evidence in the literature supporting the existence of sticking friction at the flank face of the tool (Hitomi

et al, 1962 and Trigger et al, 1952)[63]. Ham et al (1961) [64] also showed that adhesion at the flank face could be prevented by the application of a lubricant and an increase in tool clearance angle.

$$\phi = \mathrm{F}(\beta, \alpha) \tag{13}$$

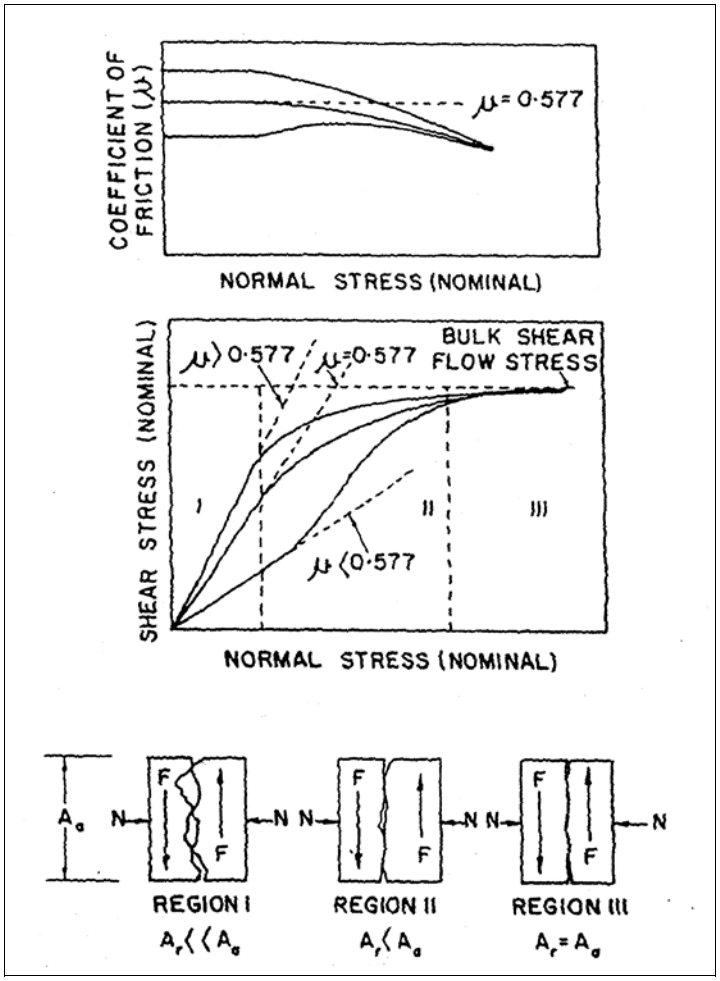

Figure 16: A schematic representation of dry friction for pressures in the metal cutting range showing that for light pressures the coefficient of friction is independent of pressure and Amontons' law applies. (As the pressure increases in clean surfaces sub-surface flow takes place when F=At and p=0.577 and F remains constant at large pressures unless t is altered by phenomena such as work hardening. p decreases with increase of pressure if t remains constant) (Thomsen, 1969) [62].

The severely work hardened chip which is formed by a shear process in the primary shear zone flows up the tool rake face under the action of large normal and shear stresses (Ham et al 1961)[64]. Assumption that the frictional condition in this region controls the geometry of the metal cutting process has led to the representation of the frictional behaviour by a single parameter β, the mean angle of friction on the tool face. β is related to the mean normal and frictional forces by the expression tan β = F/N or tan β = μ where μ is the coefficient of friction on the tool rake face. A large proportion of previous theoretical work concerning the mechanics of metal cutting has dealt with the effect of the mean angle of friction β and the tool rake angle α on the shear angle Φ.

With the above basic understanding of the orthogonal machining process, the following pages provide a comprehensive review of the various machining simulation models developed based on the FEA method starting in the early 90's.

For any FEA model there are several important parameters to be defined of which the following few play a critical role as they form the basis of the simulation.

- Material model: Represents the behavior of the material while cutting.
- Chip separation criteria: Governs the formation of the chip.
- Friction model: represents the friction at the tool - work / tool – chip interface.

Klamecki and Kim [81] studied the effects of change in deformation state across the shear zone in a chip formation process using Finite Element Modeling. A 3- D orthogonal metal cutting model was developed using sixty 20 node finite elements. Two cases were considered one with isothermal material deformation and the other including heat generation from deformation. Plastic yielding was based on the Von Mieses Yield

criterion and the simulation was stopped when the calculated effective plastic strain values reached 0.8. Results indicated that constant equivalent strain contours on the central plane in an Isothermal deformation and heat induced deformation but varied in magnitude. The changes in stress states from the study indicate that large differences in deformation behavior can occur across the shear zone due to dissipation of plastic energy with stress state. A variation in temperature was observed across the extreme plane strain and plane stress states describing the actual transition in stress states. Temperature variation in the shear zone is observed implying that work material in the plane strain region may be strain hardened whereas the material in the plane stress regions may be thermally softened.

Carrol and Strenkowski [4] in 1988 developed two FEA models of orthogonal metal cutting simulations at Lawrence Livermore laboratory. One of their models used a modified version of large scale deformation updated Lagrangian code NIKE2D to observe the forces developed during the turning of Aluminum 2024-T361using a single point diamond tool. In the second method, they used an Eulerian flow field at the vicinity of the tool work interface, modeling the work piece as a rigid - viscoplastic material. In the Lagrangian formulation the work piece is modeled as an elastic – plastic material with the chip separation criteria based on the total effective strain. The simulations were conducted at lowers cutting speeds to neglect the thermal effects and at a range of rake angles from -20° to 30° the results of which were validated against the published analytical and experimental results which compared well with each other.

Shih, Chandrasekar and Yang [5] simulated a finite element orthogonal metal cutting with continuous chip formation model including the strain rate and temperature effects in 1990. The simulation was carried out under plane strain conditions on a 1020 carbon steel work material with a chip separation criterion based on the distance between the tool tip and the nodal point connecting the two elements ahead of the cutting tool. A local and global mesh rezoning technique was applied to improve the accuracy and efficiency of the computations and the cutting and feed force from the simulated result was in an order of magnitude agreement with the experimental results. One another aspect of this simulation was its ability to display the temperature distributions, stress and strains at various points during the cutting process.

A plane strain quasi static finite element simulation of orthogonal metal cutting was carried out by Komvopoulos and Erpenbeck [6] in 1991. Cutting of of AISI 4340 steel with a ceramic coated tool was studied for which elastic- perfectly plastic and elastic plastic with isotropic hardening of the work piece material were considered. Sliding friction at the tip tool contact, built up edge formation at the tool tip and crater wear were accounted for in the model. Increased friction co efficient led to the formation of secondary shear zone at the expense of thinning of the primary shear zone. Simulations of the tool with a crater lead to distortion of stress fields at the interface, increase in magnitude of the cutting forces and resulted in thinner chip formation. The simulated results were found to be in agreement with the experimental results when using elastic – plastic with isotropic hardening and a friction coefficient of 0.5.

Zhang and Bagchi [7] in 1992 simulated the process of chip formation in an orthogonal metal cutting simulation using 2 node link elements to formulate the chip separation. An OHFC copper and 70/30 brass work material was modeled with a true stress strain curves ranging between 0 and 3. The tool and chip interaction was modeled as sliding and sticking friction models in which a constant friction coefficient was used on the sliding region and the shear strength of the work piece material was employed in the sticking region. Several simulations were carried out using tools with different rake angles, results (cutting forces, chip formation and stress fields) of which agreed with the experimental values upto 80% which was good given the assumptions and approximations of the simulation. The cutting forces predicted from their simulation were very close to the experimental values, but a very high cutting speed of 150-230 m/s used. The authors also provide a comprehensive table of various simulation works carried out between the period 1973 and 1990.

Marusich and Ortiz [8] in 1996 developed a successful finite element model for cutting AISI 4340 steel accounting for relative roles of thermal softening and friction in high speed orthogonal metal cutting. A new fracture criterion based on coalescence and void growth in conjunction with the numerical procedures for nucleating and propagating the crack through the deformed chip in a ductile material is adopted to simulate the formation of discontinuous chip. Finite deformation with rate dependant plasticity, mechanical hardening continuous meshing and remeshing, fracture and thermal conductance were other important factors considered by the authors in the simulation. The simulated results captured the experimental trends in decrease of cutting force with increase in rake angles, increase of cutting forces and temperature distribution with the

increase feeds and a very good agreement of the chip morphologies captured by the finite element model with the experimentally observed chips. They also validated their FEA results against the analytical models and concluded that the later gave just a rough estimate of the values as they do not account for certain material properties like thermal softening.

Huang and Black [9] in 1996 conducted a study to evaluate different chip separation criterion that can be used in finite element modeling of metal cutting. Four different chip separation criteria like criterion based on the maximum shear stress in the work piece element ahead of the tool tip, criterion based on the distance between the tool tip and the node immediately ahead of the tool tip, criterion based on the average maximum shear stress in the shear plane and the criterion based on the combination of the distance and the stress were considered. The authors concluded that the choice of chip separation criteria during the steady state machining did not influence the chip formation or the stress strain distributions. Authors also point out a very useful suggestion that neither of the chip separation criteria correctly predicted the incipient of chip formation and hence to study both incipient and as well steady state cutting, a combination of physical and geometric criteria is recommended and if only steady state is studied then is easier to use geometric criterion.

Large scale deformation processes in FEA are modeled based on four different techniques viz., Lagrangian formulation, Eulerian formulation and Arbitrary Lagrangian and Eulerian (ALE) formulation. [68,69]

Lagrangian formulation is one of the oldest methods used to model the metal cutting problems. In this method the mesh is attached to the material model and it deforms along with the material during the machining process. Deformation happens in time increments and after each time increments, the model is updated and the updated position acts as the initial position for the next increment. Since the mesh deforms with the material, the elements tend to distort heavily which leads to numerical instability of the analysis. Chip formation criterion is very important when modeling a Lagrangian model as it determines when the plastic deformation takes place. To avoid this drawback, a new method was developed in which the mesh was not attached to the material modeled and this method is referred to as the Eulerian formulation.

In Eulerian formulation, the mesh acts like a net allowing the material to pass through it when deforming. Eulerian method can be observed as a two step process beginning with the deformation of the material as in Lagrangian model and then mapping the deformed mesh to the fixed Eulerian mesh. This method does not require an explicit material failure criterion, requires fewer elements and lesser time comparatively and it can also capture the continuous flow of material. The main disadvantage of this method is that as the mesh is spatially fixed in this method, it becomes very difficult to obtain the data from the free surfaces and moreover it requires a customized algorithm to remesh the machined surface and as well not suitable for modeling discontinuous chip formation.

The third method is the combination of both Lagrangian and Eulerian methods, called the Arbitrary Lagrangian Eulerian method. The advantages of both the methods along with a specialized remeshing technique are used in ALE, which results in much

smoother mesh generation and very less element distortion. This method was developed first to be applied for fluid interaction problems which was later on further developed to be applied to solid mechanics, contact/ interactions and deformation problems. The only inconvenience in this method is it requires extra computational time to complete the problems but the accuracy of the results prove it worthy. Both the Eulerian and the ALE formulations consider that there exists many materials in one element whereas Lagrangian formulation strictly restricts one material to one element.

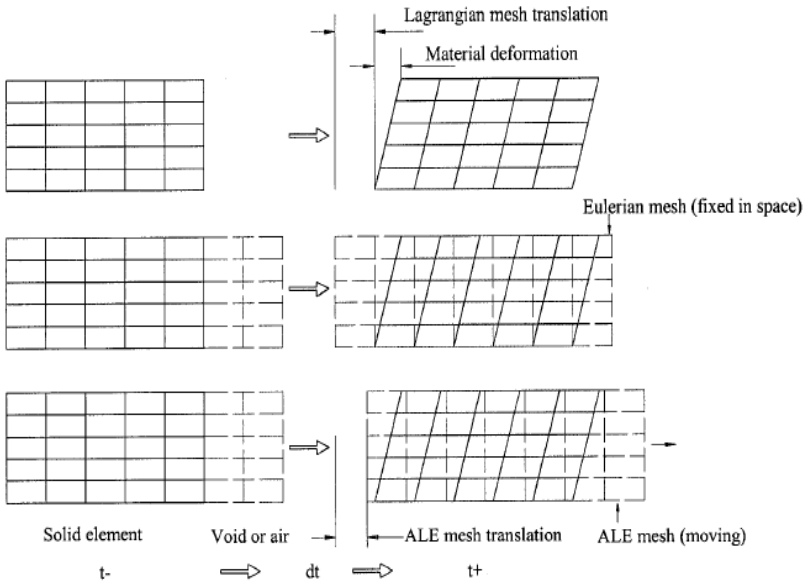

Figure 17: Comparison of Lagrangian, Eulerian, and ALE formulations [68].

There are a lot of analytical material models referred to in the literature for material modeling in FEA, but a few noted among them are Johnson-Cook model (J-C model), Oxley's model, Kinematic Plastic model and Zerrili Armstrong model.

The basic material model which predicts the behavior of the flow stress of the material based on the work hardening was proposed by Oxley [18] by the following two equations;

$$\bar{\sigma} = \sigma_0 \bar{\varepsilon}^n \tag{14}$$

$$T_{MOD} = T\left[1 - v log\left(\dot{\bar{\varepsilon}}/\dot{\bar{\varepsilon}_0}\right)\right] \tag{15}$$

Here σ_0 is the strength coefficient, n is the strain hardening index, T is temperature, v is constant, $\bar{\varepsilon}$ is strain and $\dot{\bar{\varepsilon}}$ is strain rate. This model has been employed in modeling the orthogonal cutting process of a low and medium carbon steels in conjunction with the slip line field analysis. It is also used as an analytical solution to predict the cutting forces, average strain, and strain rate occurring in the primary shear zone.

Johnson Cook [66, 72, 20] material model is usually used for high strain rate deformation dynamic problems coupled with temperature effects. The flow stress of the material is given as a product of strain, strain rate and temperature effects. The J-C model assumes that the slope of the flow stress curve is independently affected by strain hardening, strain rate sensitivity and thermal softening behaviors.

The yield stress is, therefore, expressed as

$$\bar{\sigma} = \left[A + B\left(\bar{\varepsilon}^{pl}\right)^n\right]\left[1 + C\ \ln\left(\frac{\dot{\bar{\varepsilon}}^{pl}}{\dot{\varepsilon}_0}\right)\right]\left(1 - \hat{\theta}^m\right). \tag{16}$$

Johnson-Cook strain rate dependence assumes that

$$\bar{\sigma} = \sigma^0(\bar{\varepsilon}^{pl}, \theta) R(\dot{\bar{\varepsilon}}^{pl}) \tag{17}$$

and

$$\dot{\bar{\varepsilon}}^{pl} = \dot{\varepsilon}_0 \exp\left[\frac{1}{C}(R-1)\right] \quad \text{for} \quad \bar{\sigma} \geq \sigma^0, \tag{16}$$

where

$\bar{\sigma}$ is the yield stress at nonzero strain rate;

$\dot{\bar{\varepsilon}}^{pl}$ is the equivalent plastic strain rate;

$\dot{\varepsilon}_0$ and C are material parameters measured at or below the transition temperature, $\theta_{\text{transition}}$;

$\sigma^0(\bar{\varepsilon}^{pl}, \theta)$ is the static yield stress; and

$R(\dot{\bar{\varepsilon}}^{pl})$ is the ratio of the yield stress at nonzero strain rate to the static yield stress

(so that $R(\dot{\varepsilon}_0) = 1.0$).

Apart from the flow stress model there is another J-C model that is very useful in initiation of deformation in the form of cracks and the model is usually referred to as J-C dynamic failure criterion. This model is based on the value of the equivalent plastic strain at element integration points; failure is assumed to occur when the damage parameter exceeds 1. The damage parameter, ω, is defined as

$$\omega = \sum \left(\frac{\Delta \bar{\varepsilon}^{pl}}{\bar{\varepsilon}_f^{pl}} \right), \tag{17}$$

where $\Delta \bar{\varepsilon}^{pl}$ is an increment of the equivalent plastic strain, $\bar{\varepsilon}_f^{pl}$ is the strain at failure, and the summation is performed over all increments in the analysis. The strain at failure, $\bar{\varepsilon}_f^{pl}$, is assumed to be dependent on a non dimensional plastic strain rate, $\dot{\bar{\varepsilon}}^{pl}/\dot{\varepsilon}_0$; a dimensionless pressure-deviatoric stress ratio, p/q (where *p* is the pressure stress and *q* is the Mises stress); and the non dimensional temperature, $\hat{\theta}$, defined earlier in the Johnson-Cook hardening model. The dependencies are assumed to be separable and are of the form

$$\bar{\varepsilon}_f^{pl} = \left[d_1 + d_2 \exp\left(d_3 \frac{p}{q} \right) \right] \left[1 + d_4 \ln\left(\frac{\dot{\bar{\varepsilon}}^{pl}}{\dot{\varepsilon}_0} \right) \right] \left(1 + d_5 \hat{\theta} \right), \tag{18}$$

where d_1–d_5 are failure parameters measured at or below the transition temperature, $\theta_{\text{transition}}$, and $\dot{\varepsilon}_0$ is the reference strain rate. You provide the values of d_1–d_5 when you define the Johnson-Cook dynamic failure model. This expression for $\bar{\varepsilon}_f^{pl}$ differs from the original formula published by Johnson and Cook (1985) in the sign of the parameter d_3. This difference is motivated by the fact that most materials experience an increase in $\bar{\varepsilon}_f^{pl}$ with increasing pressure-deviatoric stress ratio; therefore, d_3 in the above expression will usually take positive values.

When this failure criterion is met, the deviatoric stress components are set to zero and remain zero for the rest of the analysis. Depending on the situation, the pressure

stress may also be set to zero for the rest of calculation (if this is the case, element deletion is specified and the element will be deleted) or it may be required to remain compressive for the rest of the calculation (if this is the case, element deletion is not specified). By default, the elements that meet the failure criterion are deleted.

Zerilli- Armstrong (ZA) [66, 19] model accounts for the crystal structure of the materials based on the dislocation mechanics theory of materials. This constitutive model describes Body cubic centered (BCC) and face cubic centered (FCC) lattice structures separately in the following two equations:

$$\bar{\sigma} = C_0 + C_1 \ exp\left(-C_3\ T + C_4 T\ ln\left(\dot{\bar{\varepsilon}}\right)\right) + C_5 \overline{(\varepsilon)}^{\,n} \quad \text{(BCC)} \qquad (19)$$

$$\bar{\sigma} = C_0 + C_2 \ \overline{(\varepsilon)}^{\,n} exp\left(-C_3\ T + C_4 T\ ln\left(\dot{\bar{\varepsilon}}\right)\right) \quad \text{(FCC)} \qquad (20)$$

C_0, C_1, C_2, C_3, C_4, C_5 and *n* are empirical constants of the material which are usually determined by experience rather than using computational methods.

Kinematic hardening [70] material model is one model that accounts for hardening and plastic deformation of the material under loading, once a material is loaded, the state of stress moves outward from the yield surface causing the plastic deformation. Once plasticity sets in there are two types of hardening possible viz., isotropic hardening and kinematic hardening.

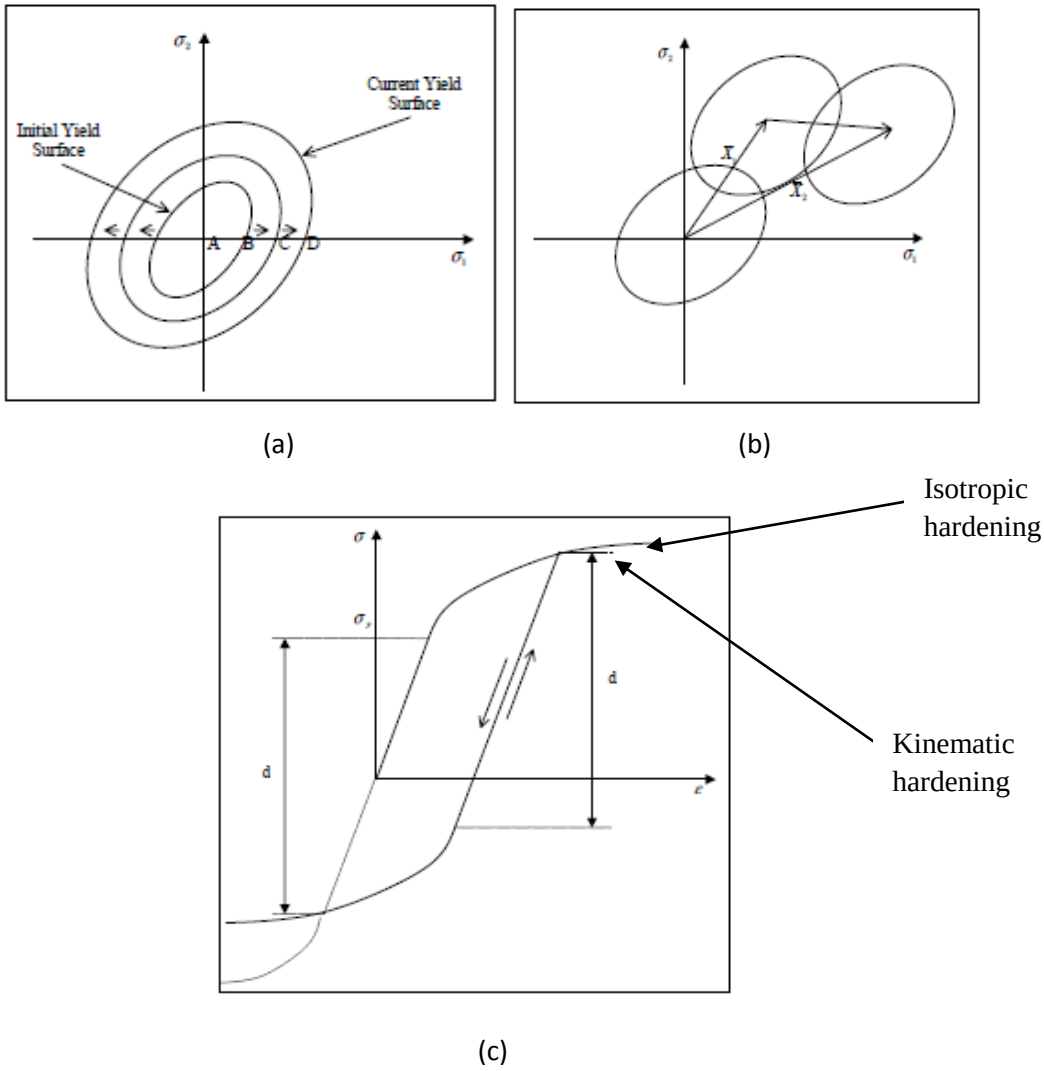

Figure: 18. (a): Isotropic hardening; (b): Kinematic hardening; (c): Stress strain curve [70]

The change in the yield surface is accounted for in the isotropic hardening case. A specimen when loaded in uniaxial tension beyond the yield stress and then unloaded and reloaded in the uniaxial compression, if a change in magnitude of the yield surface is observed without any translation then the material undergoes isotropic hardening. This is not the case with kinematic hardening where the yield surface after cyclic loading will

reduce in magnitude as well translates causing anisotropy of material which is also referred to as bauschinger effect.

The kinematic plastic behavior is represented by the following equation to model the material.

$$\sigma_y = \left[1 + \left(\frac{\dot{\varepsilon}}{C}\right)^{1/p}\right] \left(\sigma_0 + \beta\, E_p\, \varepsilon_p^{eff}\right) \tag{21}$$

Here σ_y is the yield stress, $\sigma_0$the initial yield stress, $\dot{\varepsilon}$is the strain rate of the material. Effective plastic strain is represented by ε_p^{eff}, C and P are the Cowper Symonds parameters that scales the yield stress by strain dependant factor, E_p is the tangent modulus and β represents the plastic hardening type (0 for kinematic and 1 for isotropic) [26].

Several material models were evaluated by Ozel and Karpat (2007)[66] to identify the suitable material model for formulating high strain rate metal cutting conditions. The authors combine the Johnson cook model along with the cooperative particle swarm optimization technique to investigate the high strain rate plastic deformation with thermal softening occurring during the metal cutting process. The results from the newly developed algorithm have yielded better results than the traditional curve fitting technique in identifying the constants of the constitutive models. More over the study also gives a brief review about the some of the notable constitutive models such as

Oxley' model, Johnson-cook model and Zerilli-Armstrong constitutive model which are widely used in modeling metal cutting simulations.

Marusich [10, 74] in 2001 studied the effects of friction and cutting speed on cutting force by simulating 2-dimensional orthogonal cutting of aluminum 6061-T6 in a commercial software AdvantEdge. Material model accounting for thermal softening and mechanical hardening with power law was used to model the work piece material. It was found that there occurs a transition in the basic material behavior from lower strain rate to a higher strain rate which led to the development of a two staged material model. The cutting forces and chip thickness measurements from the simulation were validated against the experimental results obtained by Kobayashi et. al., (1960) and was found to be within 10% variation and as well corresponded to the trends when the cutting conditions changed. From the temperature measurements it was observed that as the speed increases the temperature in the secondary shear zone changes dramatically while the primary shear zone temperature change is moderate indicating that the secondary shear zone plays an important role in reducing the cutting forces as a function of speed.

Arrazola, P, J., Ugarte, D., Montoya, J., Villar, A., and Marya, S.,(2005) [11] chip formation process in 2 Dimensional using the commercial FEA solver Abaqus explicit solver and AdvantEdge software. Johnson-Cook constitutive material model is used to represent the work piece and the tool is kept rigid. The chip tool interface is modeled with a constant coulomb friction coefficient and the thermal and mechanical boundary conditions are coupled using the Adaptive Lagrangian Eulerian method which also helps in reducing the distortion elements to an extent. The simulated values of the cutting

forces obtained from both the software were validated against the experimental values and it was found that the results from Abaqus was 66% and that from AdvantEdge was144% in accordance with the experimental results.

Zouhar and Piska [65] in 2004 used LS Dyna to model orthogonal metal cutting process and studied the effects of varying the tool geometry. The work material is AISI 1045 steel modeled using a Johnson-Cook constitutive material model along with a Johnson cook damage criterion to calculate the equivalent plastic strain and the flow stress of the work piece which plays a major role in plastically deforming the material. The cutting tool is modeled as a rigid body and the rake angle is varied between -5° to 10° along with three different nose radii. The cutting forces from the simulation seemed to increase with increase in both the rake angle and the nose radii though the main effect for that came from the change in rake angle. The chip thickness and the shear angle also were influenced by the increasing rake angle while increase of the nose radii resulted in more number of elements getting in contact with the tool thereby increasing the internal contact energy.

Pramanik, A., Zhang, L, C., and Arsecularatne, J, A.,(2007) [12] investigated the orthogonal metal cutting process in metal matrix composite of aluminum 6061 T6 alloy reinforced with silicon carbide particles in Ansys/LS Dyna. A kinematic plastic hardening material model was used as the constitutive model in building the work piece and also is used to calculate the yield stress based on a scaled strain rate dependant factor. The chip separation occurs based on the strain rate of the leading node, which when equals or exceeds the limiting value results in separation. The contact between the tool

and chip interface was modeled as an automatic sticking region based on the limiting shear stress values and the slip region based on the constant friction coefficient. A good qualitative agreement was observed when comparing the simulated data against the experimental results from the literature. It was also noted that the newly machined surface was under compressive residual stress and high tool wear when machining of composites is due to the constant sliding of debonded particles over the tool faces and the cutting edge.

Masillamani and Chessa (2004)[13] conducted studies to determine the optimal cutting conditions of in an orthogonal metal cutting process finite element model simulated in LS Dyna with Design of Experiments (DOE). A 3 dimensional metal cutting model was used in the study with the work piece material being aluminum 6061 T6. Lagrangian formulation along with the Johnson-Cook (J-C) constitutive model and the J-C damage criterion is used to build the model. Tool rake angle, cutting speed, and depth of cut were varied and peak temperature in the work material during the chip formation process compared well with the experiment data. From the DOE analysis, it was concluded that the most significant input factor to observe the temperature contours is the depth of cut followed by the cutting speed and then the rake angle.

Raczy, A., Altenhof, W,J., and Alps, A, T., (2004)[14] employed the Eulerian formulation to model the orthogonal metal cutting process of copper using elastic-plastic hydrodynamic and Johnson cook constitutive model to define the material behavior with a constant friction coefficient LS Dyna. From the simulation results it was seen that the hydrodynamic model predicted the results with much better accuracy then the Johnson

cook model. The hydrodynamic model predicted the chip thickness with a 5% error and the cutting forces with a13% error when comparing the simulated data against the experimental data while the J-C model predicts the forces with an error of 21%.

Villumsen, Morten, F., and Fauerholdt, Torben, G., [15] in 2008 predicted the cutting forces in an 3 dimensional orthogonal machining of aluminum 6082 T6 using LS Dyna. A simplified Johnson cook constitutive model is used to model the work piece and the contact between the cutting tool and the work piece is set up as an eroding contact. A sensitivity of the force values predicted were analyzed by changing the mesh size, mass scaling, plastic strain rate and friction between the tool and work piece. The authors concluded that finer mesh size is required for both the tool and the work piece to avoid the fluctuations in the force outputs. Friction coefficient changes between 0.1 and 0.2 did not have any significant effect on the tool. Force output was greatly influenced when the plastic strain rate was changed. By reducing the plastic strain value the forces were better predicted but the chip formation was unrealistic. For higher values of plastic strain rates the forces were over predicted but resulted in realistic chip formation.

Su, Chong., Hou, Jun-Ming., Zhu, Li-da., and Wang, Wan-shan., [16] in 2008 developed a 2 dimensional finite element model in LS Dyna to analyze the plastic deformation and chip formation during metal cutting. The work material is nickel alloy modeled based on the elastic plastic kinematic hardening constitutive model along with the Cowper Symonds model which scales the yield stress by a strain dependant factor. Adaptive remeshing method is used to remesh the zone in close proximity to the cutting tool tip to avoid distortion of elements when cutting. The tool rake angle and the friction

coefficient are varied to observe the plastic deformation energy, temperature fields and the stress. The authors conclude that the plastic deformation energy decrease with the increase of rake angle and increase with the increase of friction coefficient and also the temperature at the second deformation zone is higher than the other contact areas as most of the heat is brought away by the chip.

Simulation model of mechanism of burr formation during the cutting orthogonal machining process was developed by Yunming and Guicheng [17] using Ansys/ LS Dyna in 2008. A 2 dimensional orthogonal metal cutting model is formulated using brass as the work material and the important factor in the bur formation is proper definition of the chip separation criteria along with the friction coefficient. If the magnitude of the maximum shear stress criteria is large or if the friction coefficient is large causing sticking of the chip it will result in high distortion of elements. On the other hand too low a value for the criterion will result in crack formation rather than a chip formation. Authors conclude that the burr formation process is greatly influenced by the size of the negative deformation zone and other main factors affecting the burr formation are the depth of cut, tool nose radii, higher the magnitude of these will result in large size burr formation.

Finite Element Modeling

Finite element modeling (FEA) has been employed to solve many problems in various fields like structural, thermal, electrical, fluid mechanics separately or in combination of two or more of them. Depending on the type of analysis, size and the accuracy of the results required the computation becomes larger and more complex which no longer can be solved on paper. Several programming techniques were used in the past to solve these complex equations (based on FEA) but consumed a long time to build the model and even longer to solve it. With new developments in computer technology several standardized software are available to solve finite element problems which reduces the modeling time considerably as it eliminates the need to write unique programs for each and every scenario analyzed. The time taken to solve complex problems did not reduce until the application of super computers emerged.

Several FEA softwares are available and the choice is usually based on the ability of the software to handle the problem under the scanner. Abaqus, AdvantEdge, MARC, Nastran, LS Dyna are few of the commercially available FEA software that have been utilized in the past by researchers to model metal cutting problems. LS Dyna has been chosen for this study because it provides several material models to describe the behavior of material under study and moreover accessible to the author on campus. A simple 2 –

Dimensional model of the orthogonal metal cutting with plane strain assumption was developed in LS Dyna. Before getting into the details of the modeling it is necessary to look into the assumptions made for the study to match the actual experiments carried out at Auburn University and others to reduce the runtime without sacrificing the validity of the model. The assumptions are as follows:

1. The cutting takes place at a constant velocity of 640 RPM / 2.12 m/s.
2. The nose radius of the tool was a constant at 50 microns.
3. Tool is modeled as rigid and tool wear is neglected in this study to reduce the complexity and runtime.
4. Room temperature was assumed to be 30 degree Celsius (Room temperature)
5. A dry machining condition is considered for this simulation.
6. Homogenous material conditions are used.
7. Metric system of units (Kg, M, s, °C, N) is followed through the entire model.

The entire modeling and solving of the model can be classified into three distinct sections as Pre processing, Solving and post processing. The pre processing step involves the geometry modeling, material definition, boundary condition definition and discretization (meshing) which is then submitted to a solver which computes and outputs a set of numbers which is interpreted using the post processor. Post processor also helps in plotting different distributions and parameters with respect to time. In LS Dyna, the pre and post processor is called the LS Prepost a Graphic User interface (GUI) in which the aforementioned procedures are carried out. The pre processed file containing the key words is called the “K – file” is submitted to the solver which in this case runs on a super

computer cluster available at Auburn university. The output result is a binary file which is interpreted using the LS Prepost GUI.

Preprocessing:

The pre processing starts with building the geometry of the model, followed by meshing, definition of material property and material model, boundary condition definition and creation of output requests.

Geometry modeling:

Geometry modeling is started off with choosing the CURVE tab in the tool bar (also available under geometry menu) which provides different tools to create a point, curve or a 3 – D surface. The geometry for the problem considered involves two parts: the tool and the work piece. The tool is created using the 'LINE' option where the co ordinates for the start and end points are defined. After defining a set for each line apply button is clicked to create the line, similarly the entire work piece and the tool are modeled. The nose radius of the tool is modeled using the option 'Circular arc' by 'tangent two lines' option. The work piece and tool dimensions are given in table 1, and after each step the model is saved as a key word file or the K file.

S.No	Geometry	Dimensions
1	Work Piece	Length - 2 mm Height - 0.5 mm
2	Tool	0.5mm*0.5 mm (With tool Rake angle and Clearance angle included)

Table 1: dimensions of work piece and tool

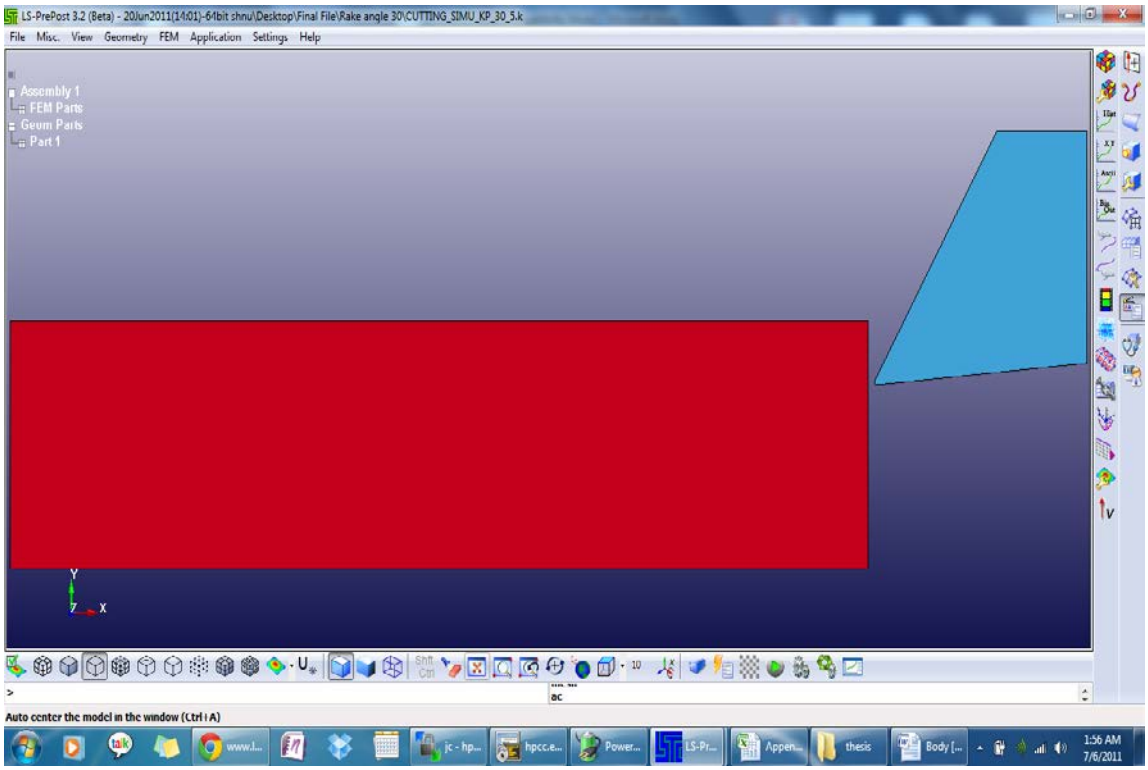

Figure 19: Screen shot from LS Dyna Showing the geometry of the tool and work piece

Meshing:

Once the geometry is completed the next important step is to mesh the model. The element type used to mesh the current model is a 2 D solid, 4 node Shell element which has been used in the literature [17, 18] to model high deformation and metal cutting problems. Since the work piece material undergoes a very high deformation at the tool cutting edge – work piece contact, that particular region of the work piece is modeled such that it has the finest mesh. Also a uniform mapped mesh is used to mesh the work piece as the distance between the successive nodes at the region of deformation is important to model the chip separation. The variable density mesh is created by splitting the line along the y axis of the work piece to the required uncut chip thickness using the

‘break curve’ option under the “CURVE” tab. This split helps in creating the fine mesh using the ‘N-line mesh’ option under “ELEMENT and MESH” tab. In the ‘N line mesh’ definition, mesh by ‘Line Sweep’ option is selected which require the selection of two lines confining the surface.

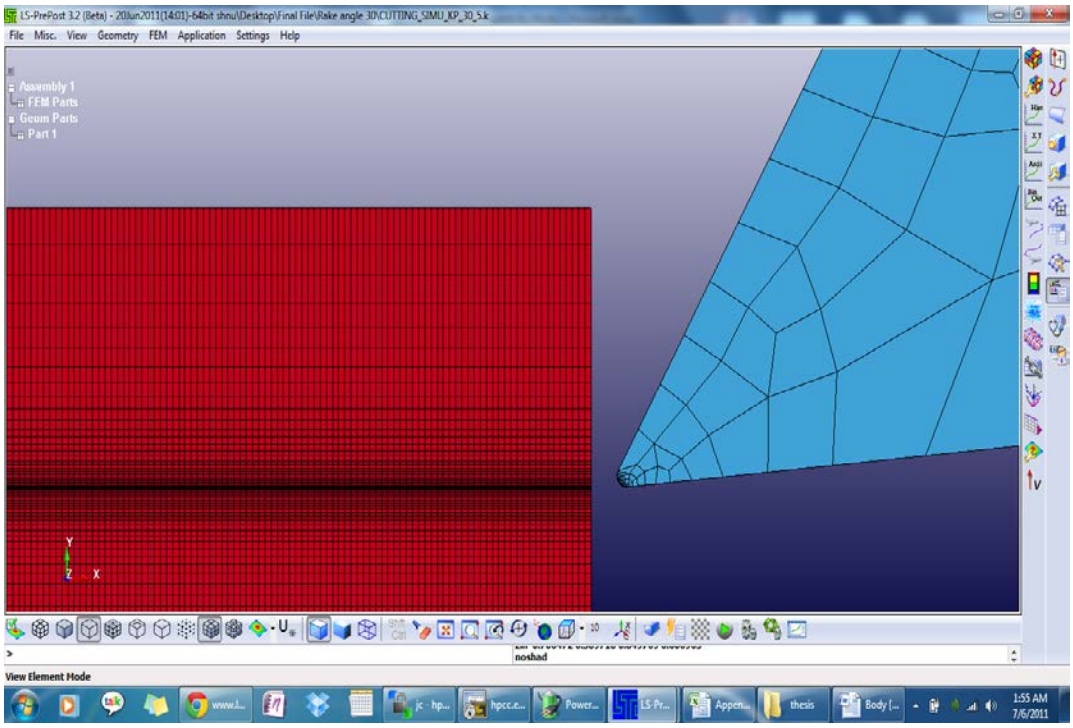

Figure 20: Screen shot from LS Dyna showing the mesh of work piece and the tool.

The bottom line and one of the vertical lines that has been split is selected, the number of nodes along each line is mentioned along with the ratio which clusters the nodes to one end of the line. The vertical line selected is meshed with a ratio, such that more nodes are present at the deformation region and the bottom line is meshed with a ratio of 1 since it does not require any high mesh density zone. Similarly the other portion of the work piece is meshed and then the split lie is merged together using the ‘merge curve’ option under the “CURVE” tab. Since two different meshes are generated, the

meshes are joined together using ‘duplicate nodes’ option under “ELMENT TOOLS” tab. The region where the separation is present is of high mesh density and so a very small tolerance value of 1 e $^{-12}$ is selected to highlight the duplicate nodes which once identified and selected, ‘Merge nodes’ option is used to merge them together.

The tool is meshed using the ‘4 line shell’ method under “ELEMENT and MESH” option by selecting all the four confining lines of the tool. Since the tool is considered a rigid body, meshing of the tool is of least importance except for the nose of the tool which gets into contact with the work piece. This region is finely meshed by increasing the node ratio of the region and the other regions are coarsely meshed (non uniform mesh) with the same element type used for the work piece. A total of 44,000 nodes are present in the work piece and approximately around 300 nodes in the tool.

The element type is defined from ‘Define’ in ‘Key word Manager’ option under the “PART and MODEL” tab. Section ‘Shell’ is selected, and the element type ‘ELFORM’ is set to 13 corresponding to a plane strain formulation and number of integration points ‘NIP’ as 4. ALE formulation of the same element is defined by setting the value of ‘SETYPE’ to 3.

Material model:

The model under study is built with two different materials: the work piece and the cutting tool. As mentioned earlier the tool is modeled rigid with a high value of elastic modulus and the material model used to define the behavior of work piece is

plastic kinematic hardening model available in LS Dyna. This model predicts the yield stress behavior of the material based on the governing equation given below

$$\sigma_y = \left[1 + \left(\frac{\dot{\varepsilon}}{C}\right)^{1/P}\right] \left(\sigma_0 + \beta E_p \varepsilon_p^{eff}\right) \tag{22}$$

The material used for work piece is Aluminum alloy Al 6061-T6 which is a commonly used material in the aerospace industry and was used while conducting orthogonal tube turning experiments at Auburn University. Khan, Akthar, S., Pandey, Amit., and Stoughton, Thomas., (2010) [23] have carried out studies to determine the characteristics of strain hardening of AL 6061 and have concluded that the material exhibits a kinematic hardening under compression. Hence the hardening type considered for this model is a kinematic linear model with an effective plastic strain value of 1.15 at strain rate of 10^4 s^{-1} taken from the work of Lesuer, Kay and LeBlanc [21].

Cowper Symonds coefficient values are taken from the work of Altenhof and Ames [22]. The material properties [75] of the tool and work piece are defined in LS Dyna using the 'Material model' option under 'Key word Manager' in the "PART and MODEL" tab. The chip formation criterion is based on the effective plastic strain value and once the element in the work piece reaches this threshold value, is deleted, leading to the separation of work material as chip.

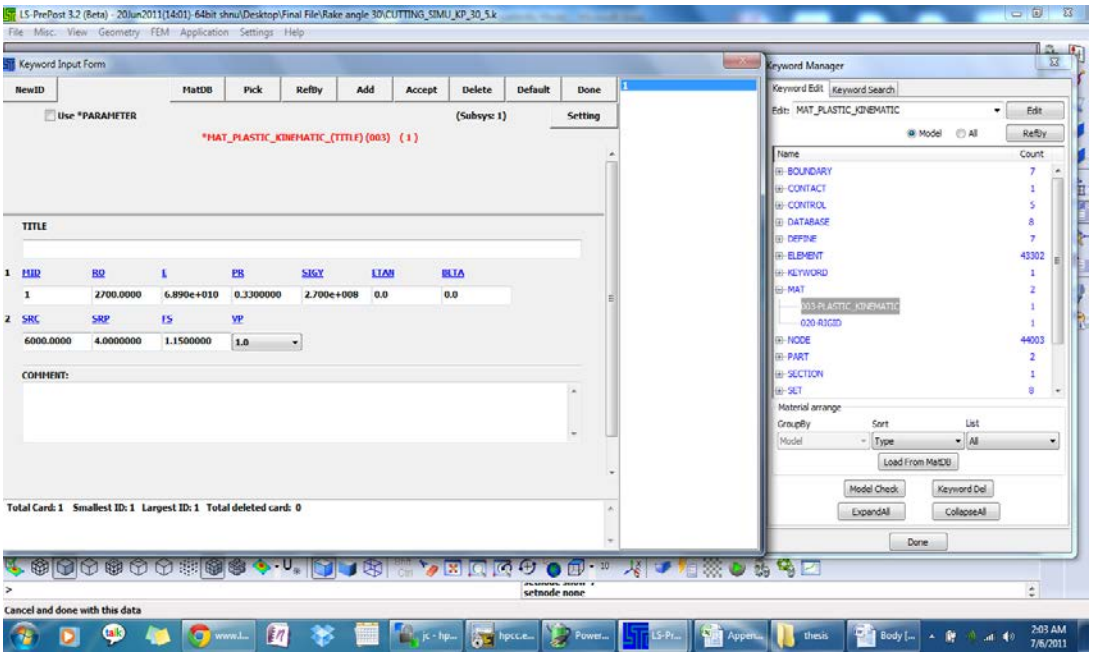

Figure 21: Screenshot from LS Dyna Showing the Material property definition Card.

Before proceeding further to define the boundary conditions and other parameters it is necessary to define node sets which makes it easier to pick up boundaries or contact surfaces while defining the remaining parameters. This can be done by getting into the “PART and MODEL” tab, selecting ‘create entity’ in which ‘set data’ is selected and then ‘set nodes’ is used to define a set of nodes which are picked from the geometry. The tool should be given a part ID which is used to define other input conditions. This is done by selecting the option ‘Set part’ instead of set node in the procedure described above. Similarly other node sets are created which are used in further defining the boundary conditions and output requests.

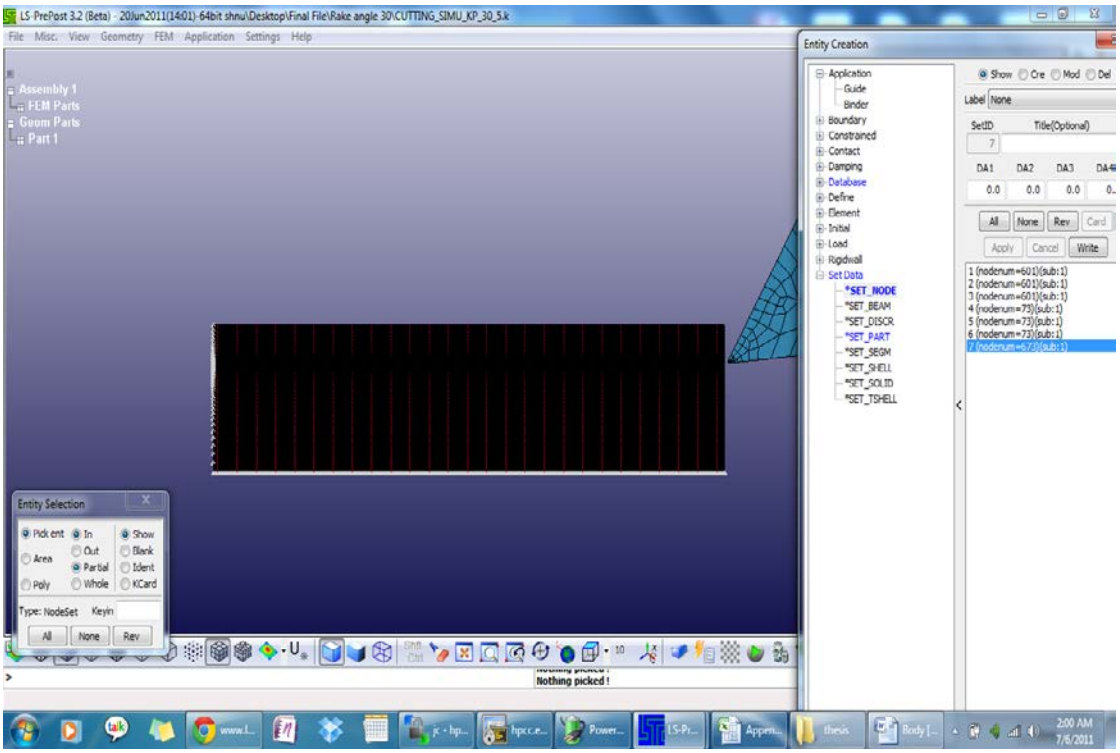

Figure 21: LS Dyna screen shot to demonstrate node set creation

Boundary conditions:

In the current model, the work piece is fixed at a certain point and the tool is moved towards the tool at a constant velocity. Since the work piece is fixed completely, all the degrees of freedom are arrested including translational and rotational. The tool degrees of freedom (DOF) are also completely arrested for in all directions except for translational motion in x direction. The boundary conditions are created by getting into the “PART and MODEL” tab and selecting the ‘Keyword Manager’ in which ‘boundary’ tab is selected. ‘Prescribed_motion_rigid’ is selected for the work piece in which all DOF are constrained by selecting a value of ‘7’ for parameter “LCID”.

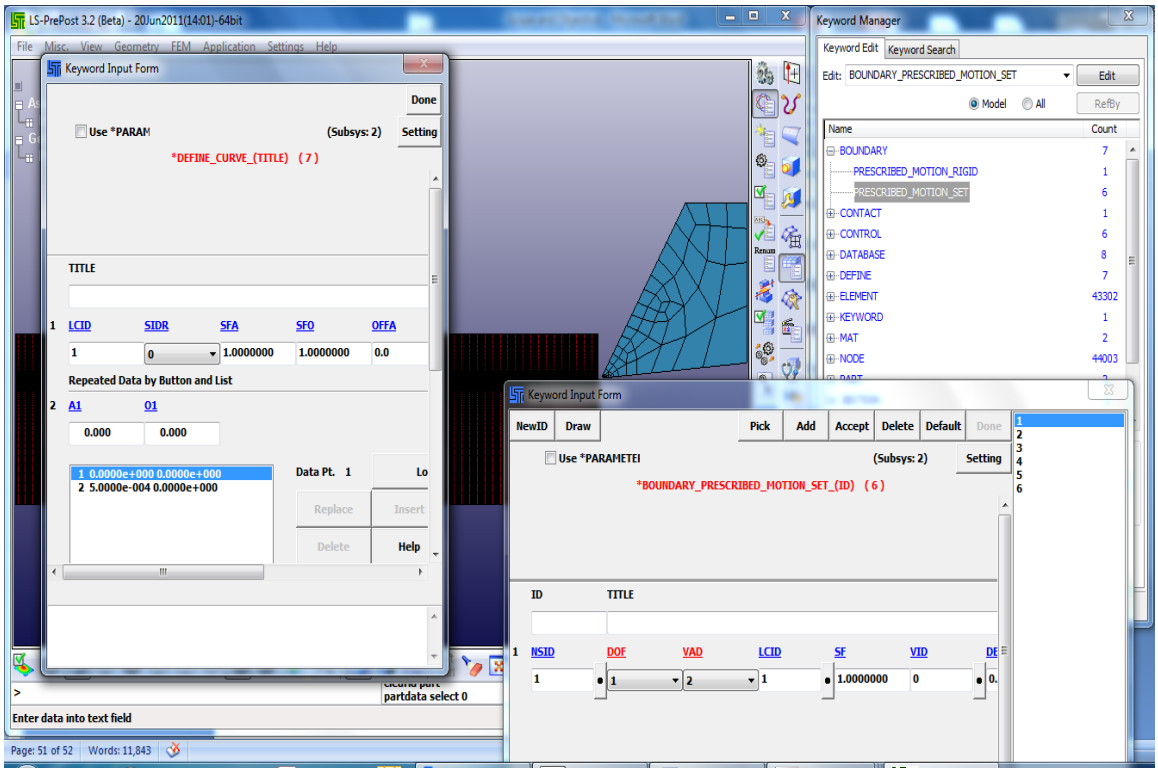

Figure 22: LS Dyna screen shot of defining boundary conditions.

Similarly for the tool motion, ‘Prescribed_motion_set’ is selected’ in which “DOF” is set to a value ‘1’ and “VAD” to a value of ‘2’meaning translational motion with a velocity in X direction. The parameter “LCID” is set at ‘1’ which corresponds to magnitude of velocity of the tool, represented by a curve for displacement against time. While fixing the work piece boundary condition, only the node set corresponding to the bottom surface, and the left vertical set of the work piece are selected from the previously defined node set ID’s

Contact and friction modeling:

A 2 D automatic single surface contact type is used to define the contact between the tool and work piece wherein the software automatically identifies the surfaces coming

in contact and assigns the surface that has more number of nodes and that undergoes large deformation as master surface and the other as slave surface. The friction between the contacting surfaces is treated as a constant coulomb friction for the current analysis and does not involve slip and stick type friction which happens in the real scenario to reduce the complexity of the model and run time. The friction coefficient values are calculated based on the Merchant's model using the experimental data obtained from orthogonal tube turning experiments conducted at Auburn University.

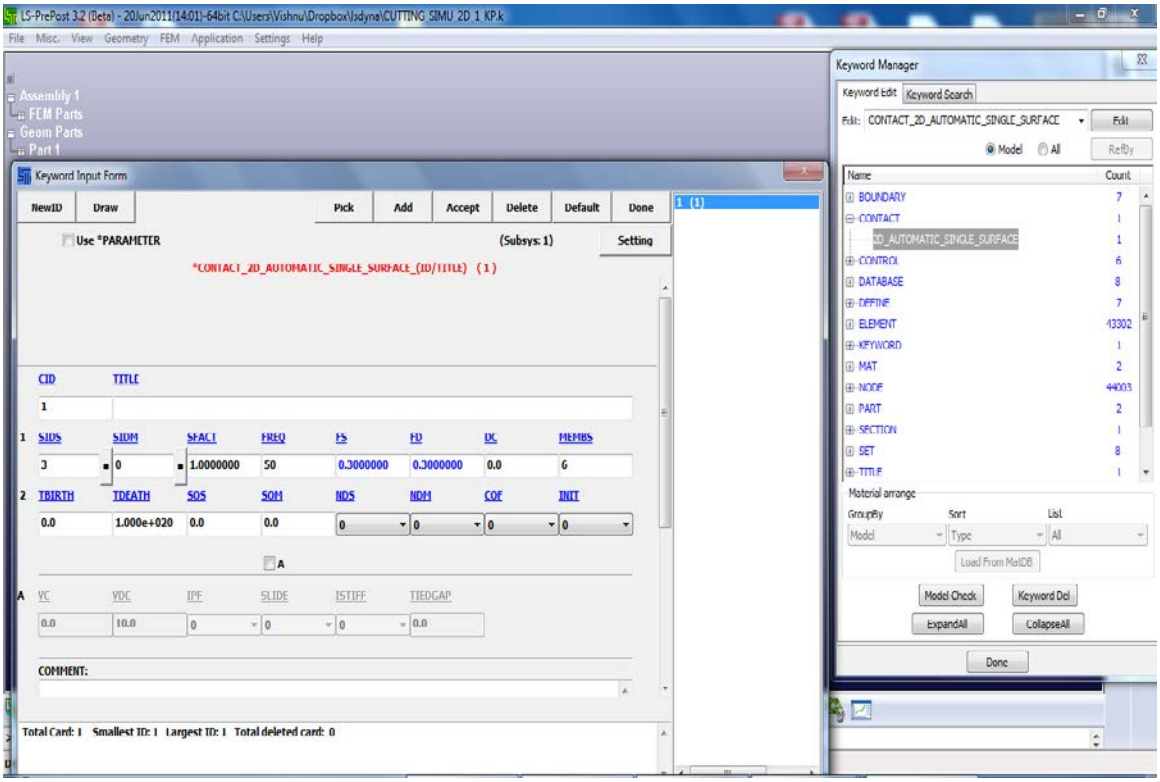

Figure 23: Screen shot from LS Dyna showing the contact type definition.

The contact is defined in LS Dyna by selecting the "PART and MODEL" tab in which 'Key word Manager' is selected, from which the '2-Automatic single surface contact' is selected from under 'Contact' option. In the contact card the values for 'FS'

and ‘FD’ are set to the corresponding friction coefficient, in the present case both are set to a equal value which enables the software to interpret that only constant friction takes place. The contact algorithm used fin this model is called the single surface contact algorithm with bucket sort to handle metal formation problems [73].

Control:

‘Control’ can be accessed from the ‘Key word Manger’ under “PART and MODEL” tab. Different types of control options are required in order to successfully run the simulation a few of which require for the current problem that can be defined under the ‘Control’ option are as follows:

1. Contact control: All the parameters in this card are set to default values except “SLSFAC” which is set to 1 is the scale factor for sliding penalties.
2. Hourglass control: All the values are set at default.
3. Shell control: All the values are set to default except “NFAIL1” and “NFAIL4” both of which are set to 1. This enables the deletion of highly distorted elements which are ‘under- integrated’ and ‘fully-integrated’ respectively.
4. Energy control: All the values are set to default.
5. Termination control: All the values are set to default except “ENDTIM” which is set to 5 e-4 is the time at which the program terminates.
6. Time step control: All the values are set to default.

This ends the modeling portion of the pre processing stage. Next important step is to define the output requests which enables in getting the plot for force values.

Output requests:

LS Dyna does not have the automatic capability to output the force values for a 2 Dimensional problem, since plotting the forces is one of the objectives of study; it has to be manually done. The tool in the current study is modeled as a rigid body and is not possible to obtain the force values acting on it, so the nodal reaction forces exerted by the work piece which is equal in magnitude but opposite in direction are obtained from the nodes on the edges of the work piece. To obtain the nodal reaction forces, the software needs to be manually told to output the forces from the required node sets or else it will output all the forces from which it will be really tedious to filter out the nodes of interest and is also a time consuming process.

Output requests are placed through the 'Database' option in the 'Key word manager' accessed through "PART and MODEL" tab. In the Database option, following are defined:

1. ASCII option: Choose "NODFOR" and set the value for "DT" to 5 e-7 which is the time interval between each output of force values.
2. Binary- D3Plot: Set the value of "DT" to 1 e-6 which is the time interval between outputs. Set all other values to default.
3. Nodal force Group: Set the value of "NSID" corresponding to the node set ID defined before for which the force values are to be output. Set all other values to default.
4. Extent-Binary: Set all values to default.
5. Format: Set all values to default.

Simulation:

In the current study, as mentioned in the objectives it is intended to study the variation of forces in metal cutting when tool rake angle and uncut chip thickness are varied. 4 different tool rake angle values of -10°, 0°, 15° and 30° which is same as the ones used in the experiment are modeled along with 5 different uncut chip thickness of 0.001”, 0.002”, 0.003”, 0.004” and 0.005”.

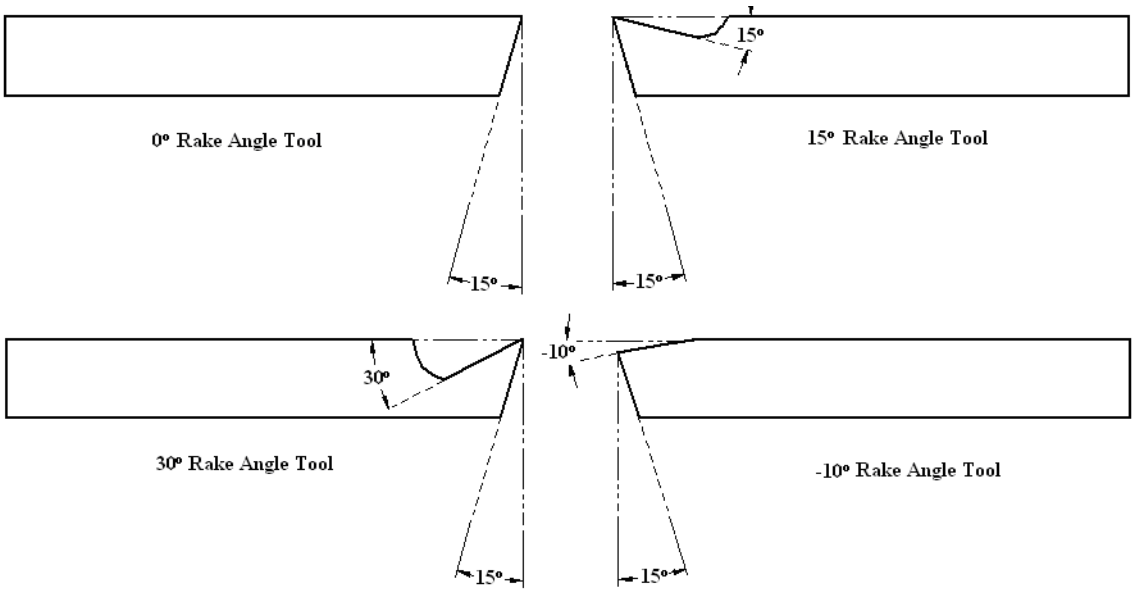

Figure 24: Tools with different tool Rake angles [71].

20 different simulations are modeled separately for each of the combinations mentioned above are built in the preprocessor and were saved as key word file (.k file). These .k files were then uploaded to the solver running on the super computer to obtain the results.

Convergence Test

In any finite element modeling and analysis, it is important to perform a convergence study to determine the number of elements or the fineness of the mesh that can be used to model the simulation to obtain close to accurate results. In this study a convergence test was carried out on a randomly chosen combination of a 30° rake angle tool at 0.005” of uncut chip thickness. Five different simulations were carried out by varying the number of nodes for each case. The force results obtained from the simulation were plotted against the number of nodes and the pattern of force variation was studied.

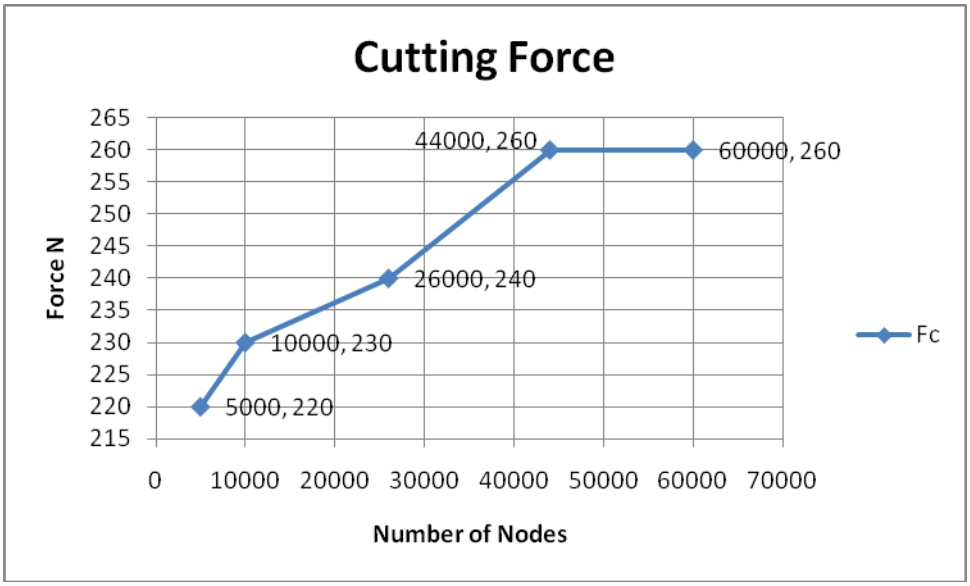

Figure 25: Convergence plot for Cutting Force.

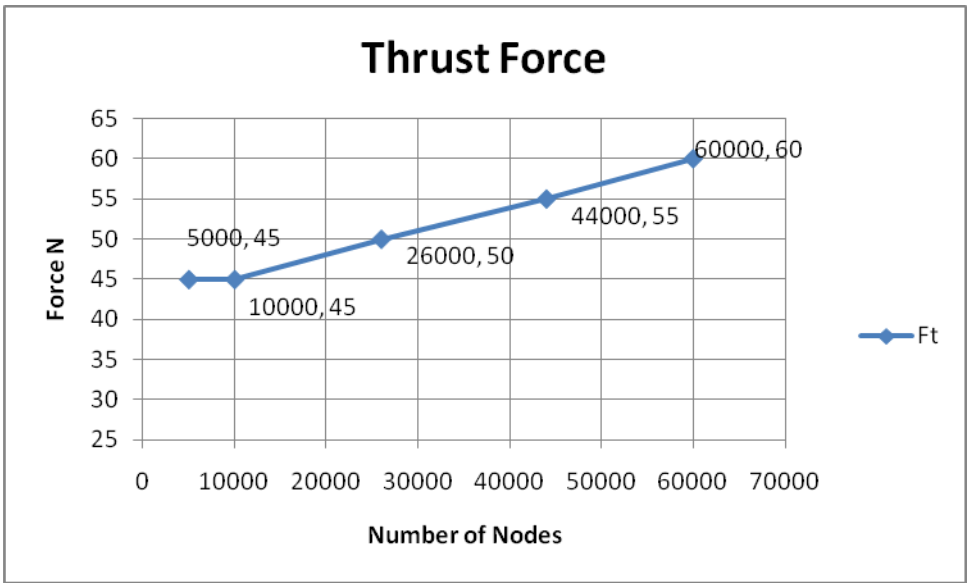

Figure 26: Convergence plot for Thrust force.

From the data it is inferred that the most accurate result is obtained when running with 60.000 nodes closely followed by the values form the simulation with 44,000 nodes. There is no change in cutting force values when run at 60,000 nodes or at 44,000 nodes and the change in values for the thrust force for the same scenario is small. Moreover the time taken to run the simulation with 60,000 nodes was upto 48 hours on a super computer, compared to the simulation with 44,000 nodes which takes less than 24 hours to complete. Hence the model with 44, 000 nodes was used for simulating all the cases.

Results and Discussions

The simulation model now enters the final phase of processing which was done by LS PrePost, post processor. The outputs from the solver were in the form of binary plots and these were imported in to the post processor using the option, “File- Open- LS dyna Binary plot”. The simulation results were animated using the play tab at the bottom tool bar. To obtain the fringe patterns of various parameters of interest, “POST” tab in the tool bar was selected, and enabling the ‘Fringe Component’ option under it. From the drop down menu, contours of Von Mises stress, Tresca maximum shear stress, plastic strain, etc., can be plotted and animated.

The forces were stored in a separate folder called “nodfor” which was accessed by selecting the ‘ASCII’ option in the “POST” menu toolbar. The forces in X and Y direction were plotted in a separate popup window which has several tools to edit the curves plotted. The curve file data was stored in an excel (.csv) format so that it could be used for further analysis using the ‘Save’ tab in the plot window.

The simulation results of 20 different combinations were animated to see the stress, strain distributions and the force values in both X and y direction were plotted. The force in z direction was checked and was found to be at zero which validates the plane strain assumption made earlier. There was a lot of noise/vibration observed in the

force values that were plotted from the LS Dyna plot and so a curve fitting for the data was made to obtain an average value for comparison purposes. The element deletion criterion for highly distorted elements was set based the plastic strain value mentioned in the input and the time taken for the tool to move forward one an element in contact was deleted, a drop in force value was observed. The noise/vibration in the output is mainly because of the fore mentioned scenario occurring frequently, leading to loss of tool work piece contact.

Similarly the force values for other combinations were obtained and two sets of plots were created. In the first set of plots, the rake angle is kept a constant and the uncut chip thickness is varied to document the variation of cutting force and thrust force. A comparison on the trend of variation of the forces obtained from simulation against the experimental data for the same condition. Second set of plots are similarly constructed but uncut chip thickness is kept a constant while the tool rake angle is varied to observe the variation of the cutting force and the thrust force. A comparison of the trends in variation of forces between the simulated and experimental results is also carried out in the second set of plots.

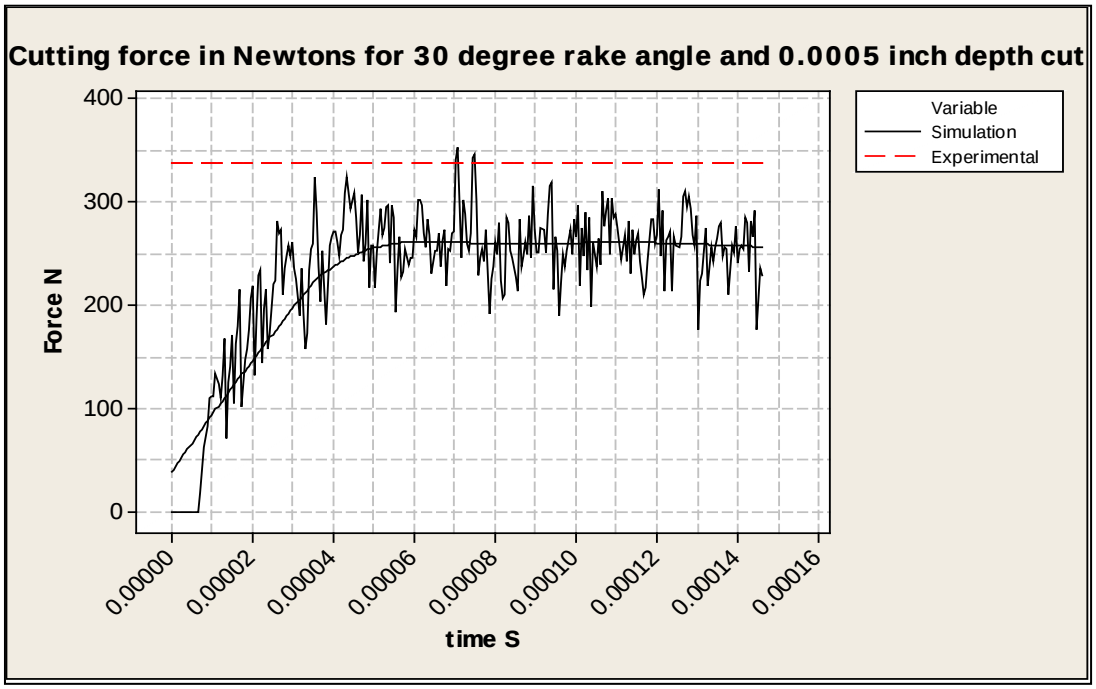

Figure 27: Comparison plot of Cutting force F_c against time.

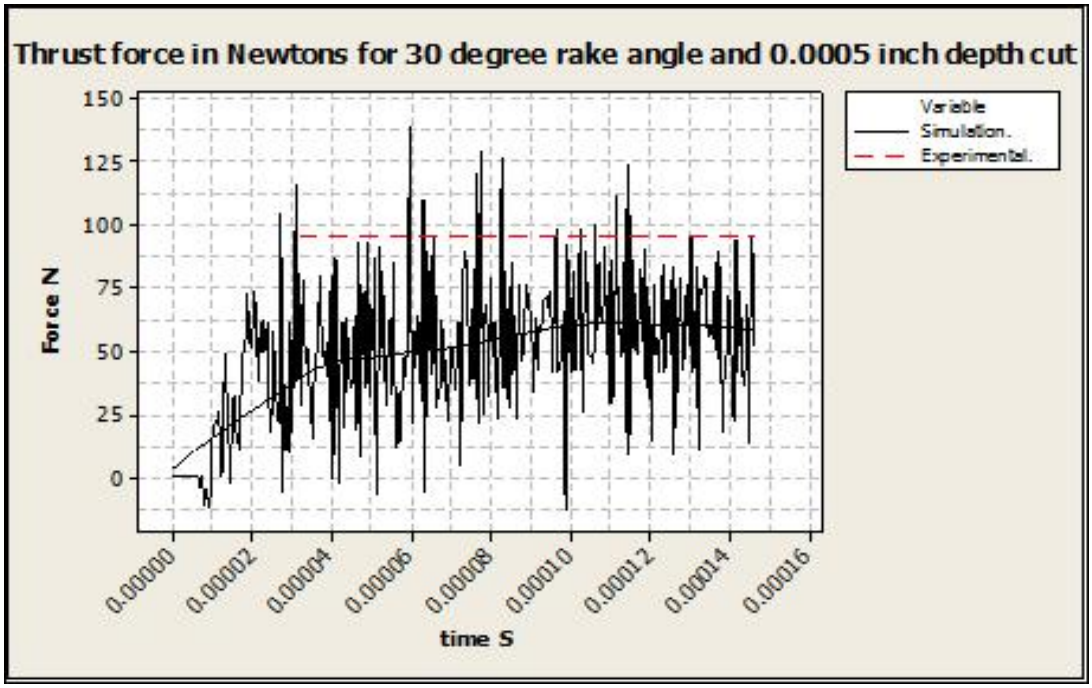

Figure 28: Comparison plot of Thrust force F_t against time.

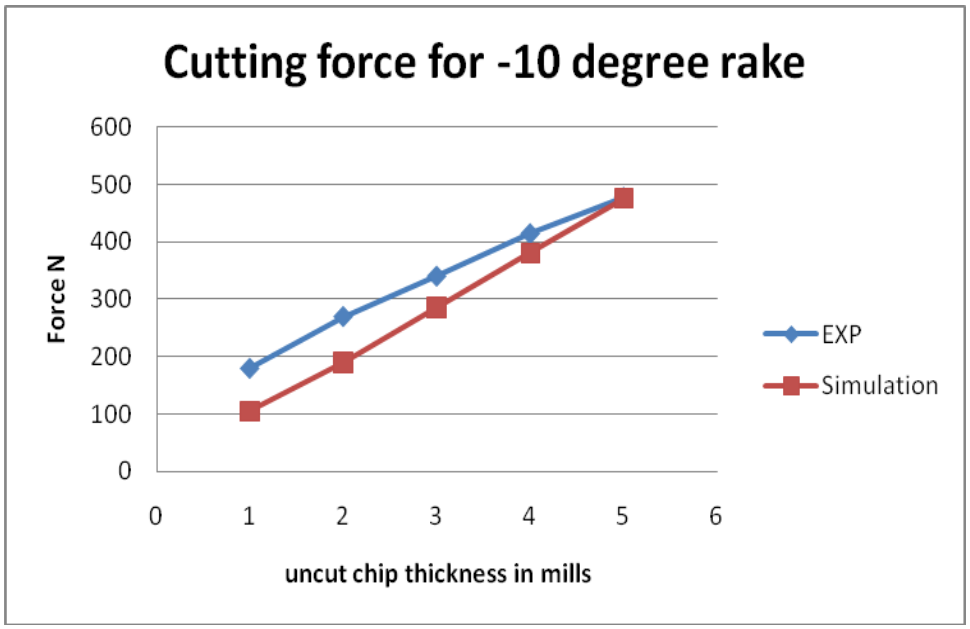

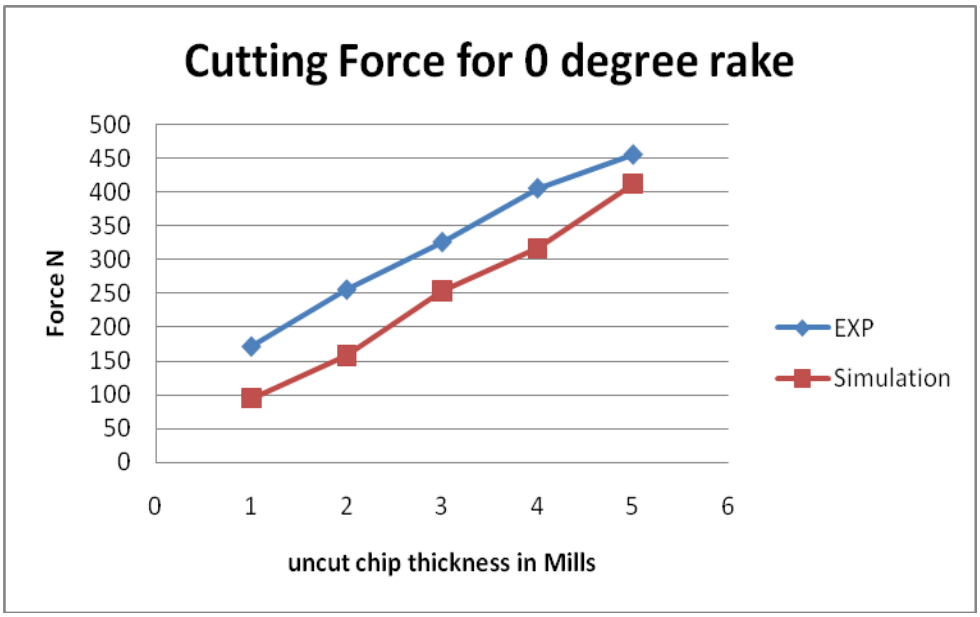

Figure 29 (a): Comparison plots for cutting force against uncut chip thickness with constant tool rake angle of -10° and 0°.

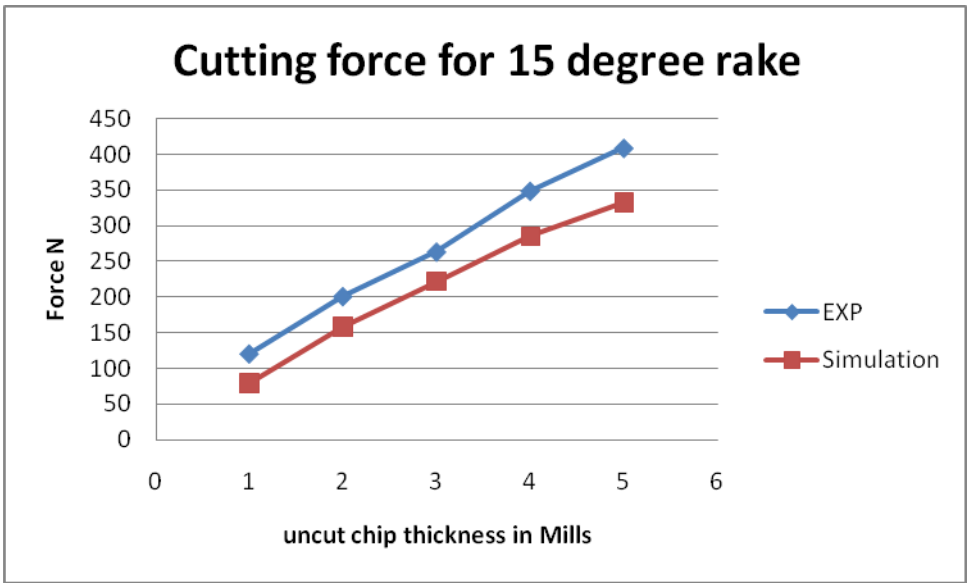

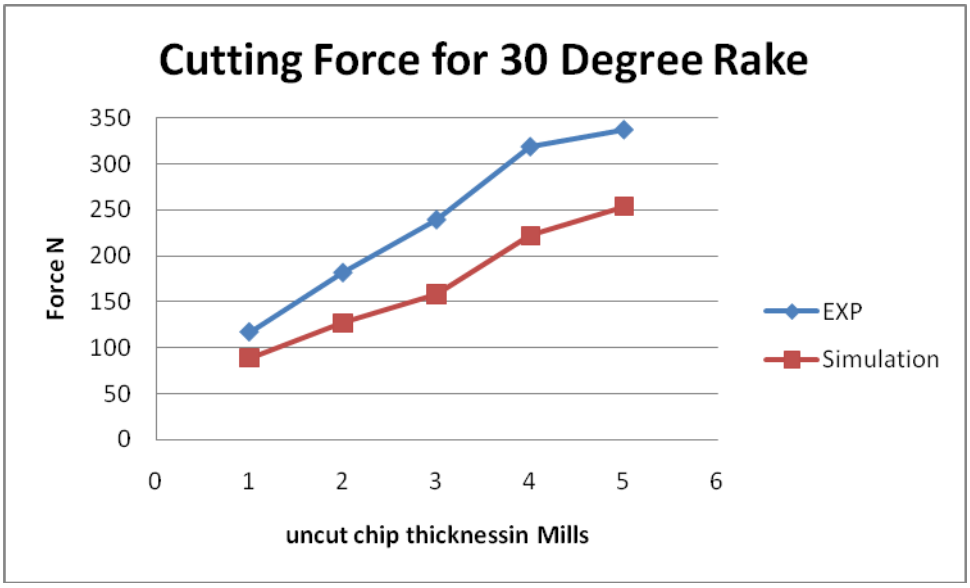

Figure 29 (a): Comparison plots for cutting force against uncut chip thickness with constant tool rake angle of 15° and 30°.

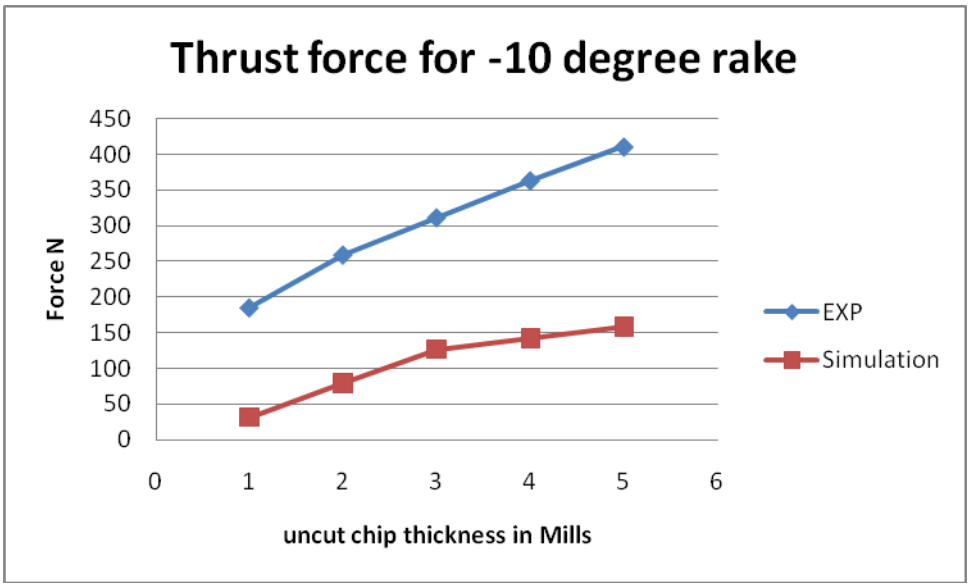

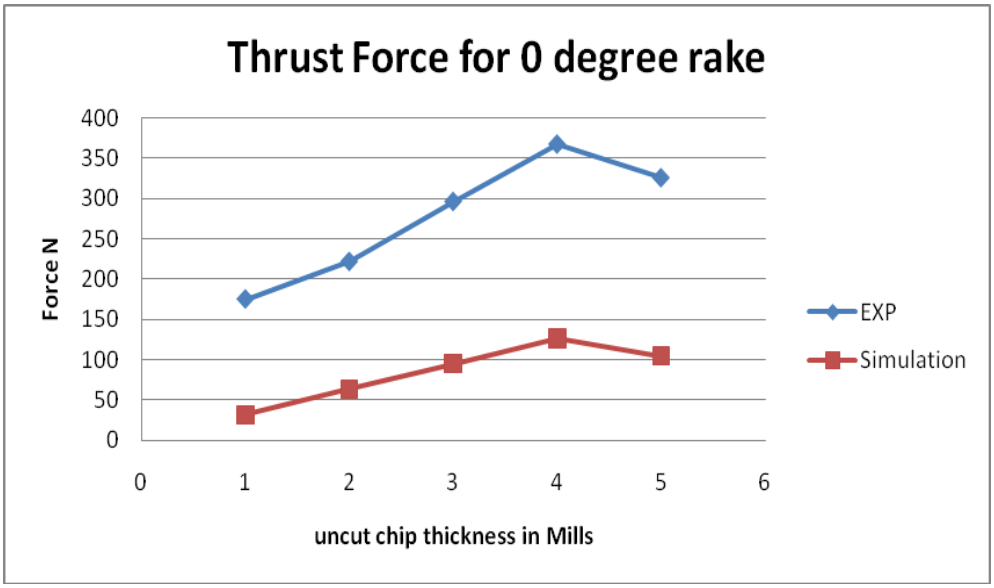

Figure 30 (a): Comparison plots for thrust force against uncut chip thickness with constant tool rake angle of -10° and 0°.

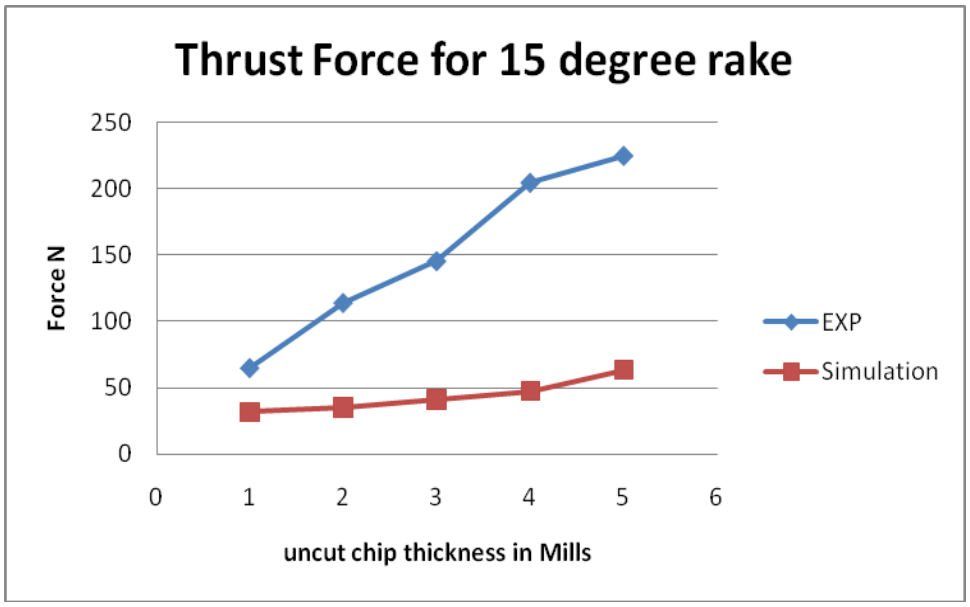

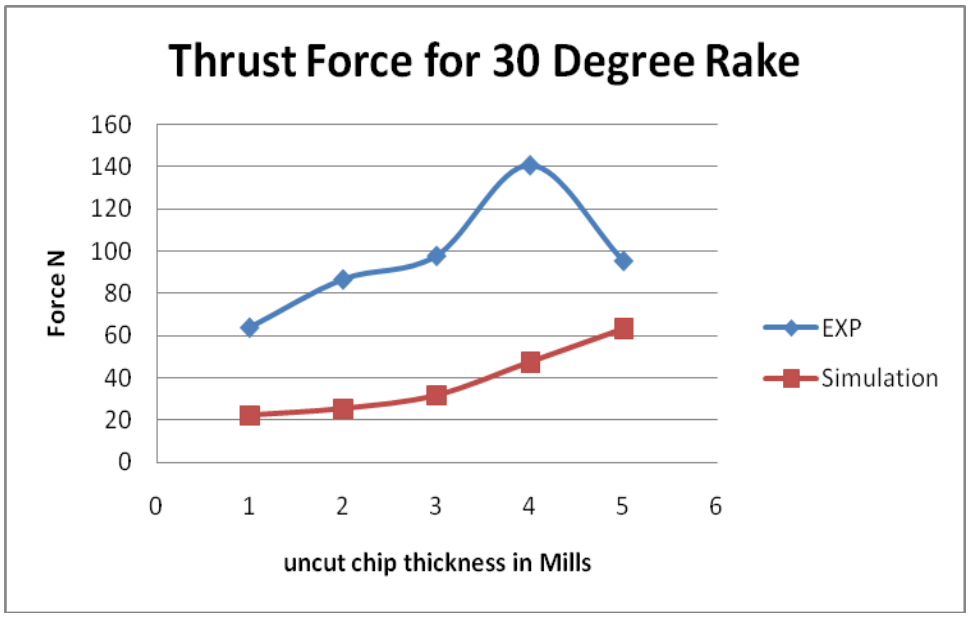

Figure 30 (b): Comparison plots for thrust force against uncut chip thickness with constant tool rake angle of 15° and 30°.

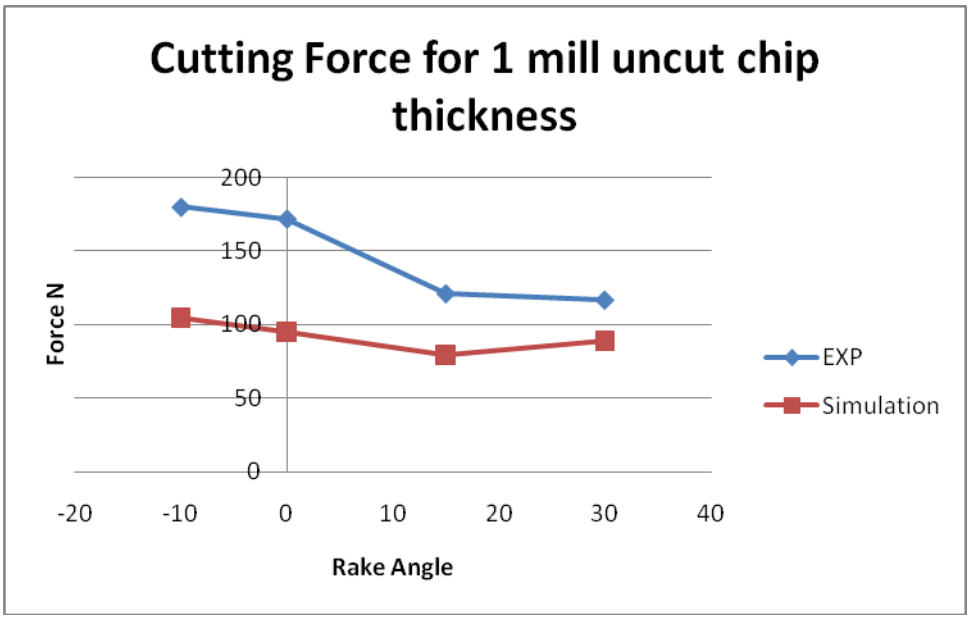

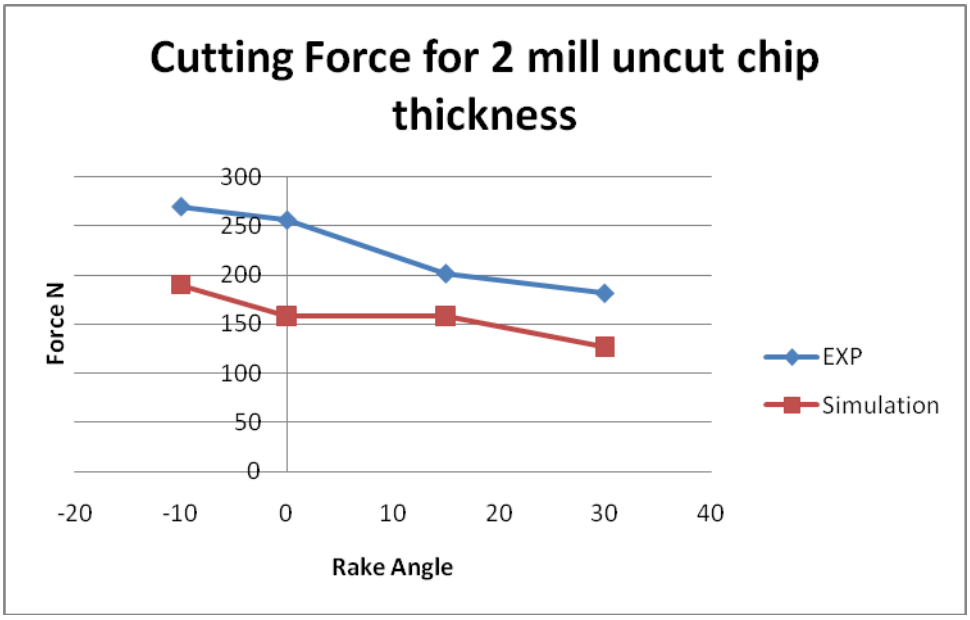

Figure 31 (a): Comparison plots for cutting force against tool rake angle with constant uncut chip thickness of 0.001” and 0.002”.

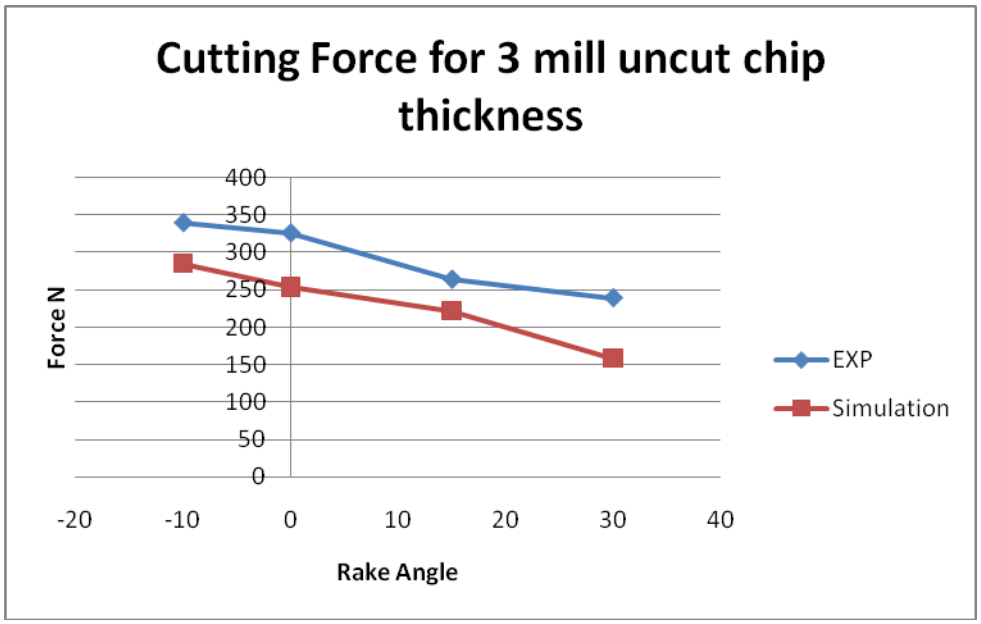

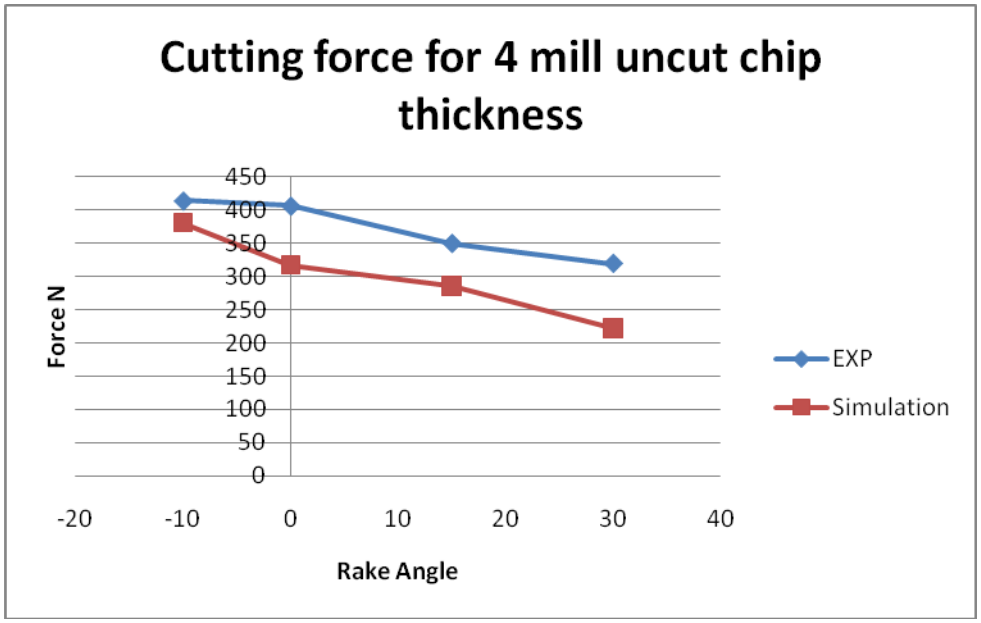

Figure 31 (b): Comparison plots for cutting force against tool rake angle with constant uncut chip thickness of 0.003” and 0.004”.

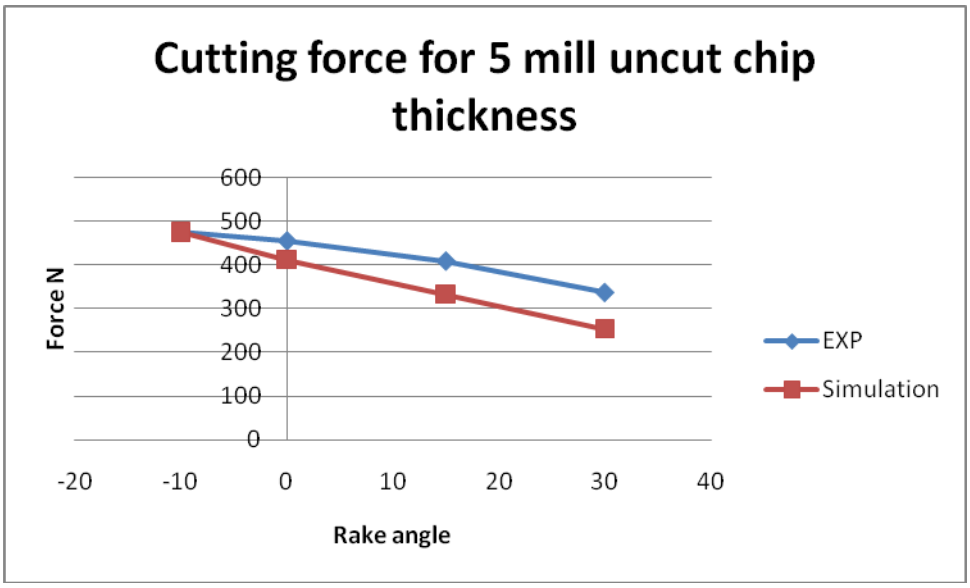

Figure 31 (c): Comparison plots for cutting force against tool rake angle with constant uncut chip thickness of 0.005".

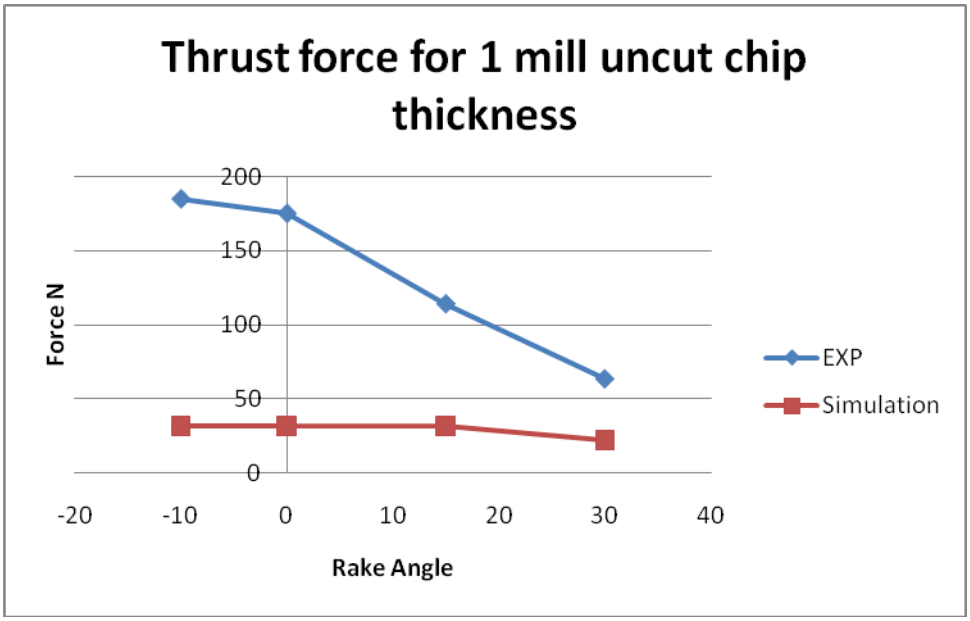

Figure 32 (a): Comparison plots for thrust force against tool rake angle with constant uncut chip thickness of 0.001" and 0.002".

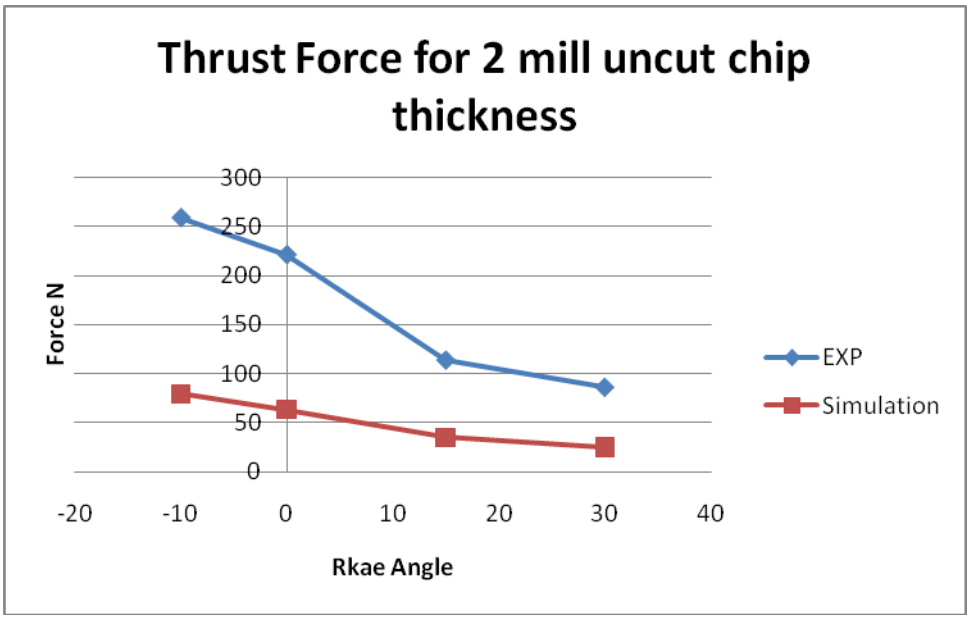

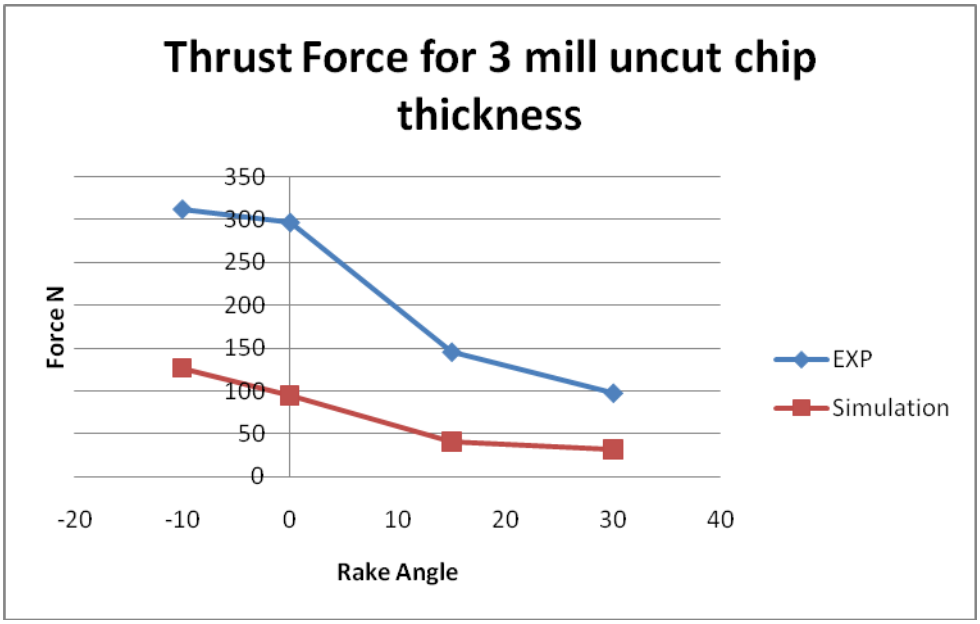

Figure 32 (b): Comparison plots for thrust force against tool rake angle with constant uncut chip thickness of 0.003” and 0.004”.

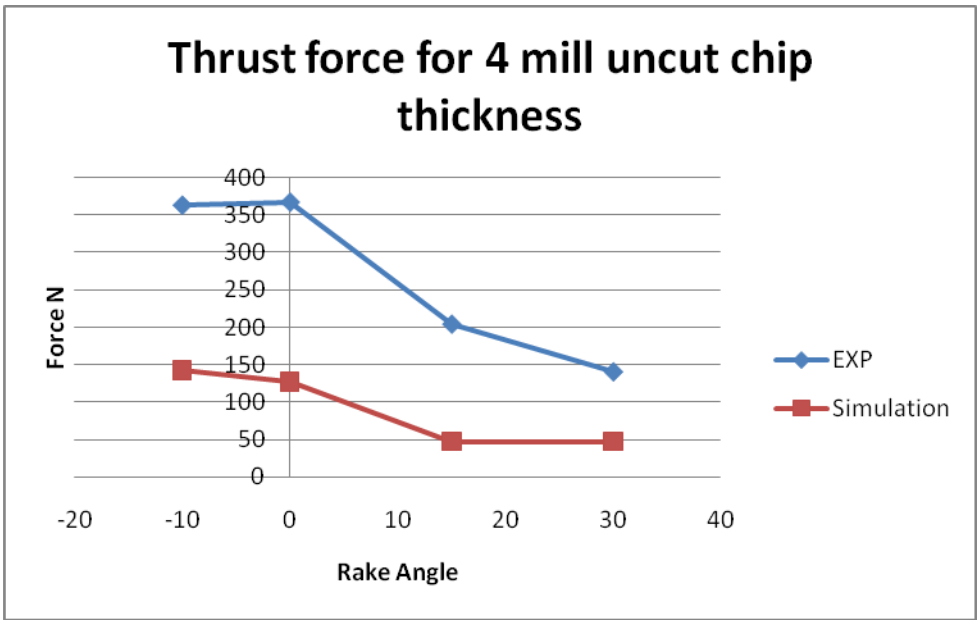

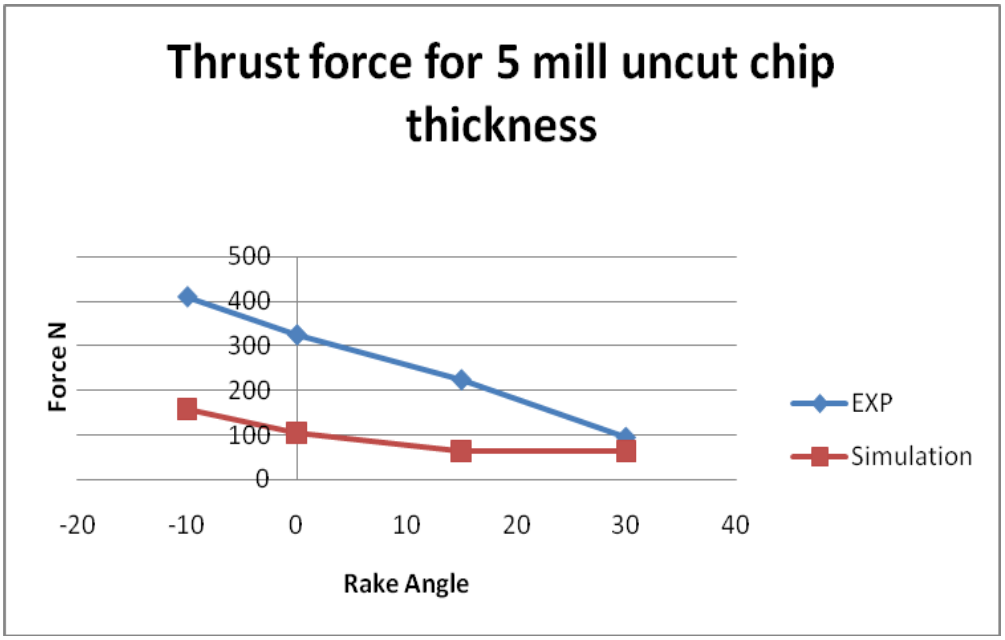

Figure 32 (c) : Comparison plots for thrust force against tool rake angle with constant uncut chip thickness of 0.004” and 0.005”.

From the above graphs, following were inferred:

- The cutting force and the thrust force predicted by the simulations were under estimated values when compared to the experimental results as shown in figure 27 and figure 28. The cutting force values were under estimated by a small percent but the thrust force values were much smaller in comparison with the experimental values.

- In figure 29, the graphs showed that when the rake angle was maintained a constant, the cutting force increased with the increase in uncut chip thickness, which was the in good agreement with the trend observed with the experimental results even though the magnitude was not the same.

- From the graphs in figure 30, an increase in thrust force was observed with increase in uncut chip thickness for constant tool rake angles. The trends in variation of the simulated results were similar to that observed during the experiments, but again, the magnitudes of the simulated results were too low.

- A couple of unusual observations were made in the graphs in figure 30, first in the case of a -10 degree rake angle tool, the thrust force variation for uncut chip thickness of 0.003", 0.004" and 0.005" was very low, when compared to the experimental results which showed a uniform increase.

- In figure 30, the graph of thrust force for 30 degree tool rake angle, the simulated values show a trend of increasing nature with for all uncut chip thickness which

had a contradiction with the experimental value in just one instance of 0.005” uncut chip thickness were the experimental value dropped down.

- When the uncut chip thickness were kept constant, the cutting forces decreased when the tool rake angle changes from a negative to positive as plotted in the graphs in figure 31. Decreasing trend of the simulated results was in good agreement with the trend of the experimental data but varied in magnitude.

- The graphs in figure 32 shows a decreasing trend of the thrust force when the tool rake angle was changed from a -10° to 30° for constant uncut chip thickness. A similar trend in variation of the thrust forces was observed in the experimental results, but again the magnitude of the simulated results being small.

- One major variation observed was with the simulated thrust force values not decreasing uniformly between a 15 degree tool and a 30 degree tool for a constant uncut chip thickness, the variation was almost nil for a 0.004” and 0.005” uncut chip thickness. This was not the case with the experimental results were the drop in thrust force values between 15 and 30 degree tool rake angles were uniform as seen in figure 32.

- Another contradicting observation in figure 32 was the plot for a 0.001” uncut chip thickness, the thrust force values simulated even though exhibited a decreasing pattern as that of the experimental values, the magnitude of change was very low as compared to the largely decreasing experimental results.

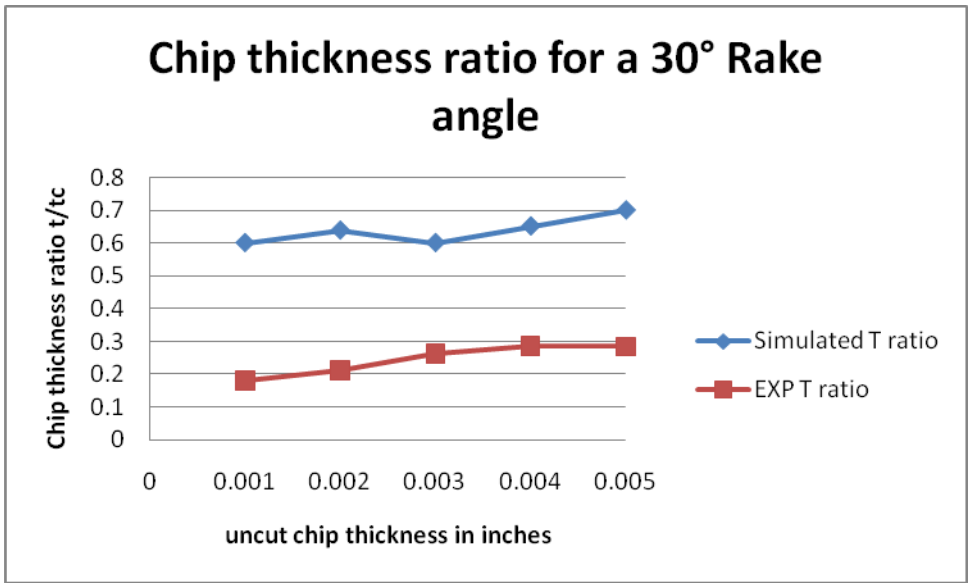

Figure 33: Comparison plots for Chip thickness ratio t/tc against uncut chip thickness at constant tool rake angle.

Although the plots comparing the forces against different rake angles and uncut chip thickness show a good agreement in the variation trend with the experimental values, the magnitude difference is high especially for the thrust force values. The primary reason for such observation can be attributed to the limitations of modeling metal cutting problems using finite element analysis software which is given below.

- It was not possible to maintain the tool work piece contact, at the point of cutting at all times in the current model. The reason being that, in the current model the chip separation takes place based on the failure strain specified in the input. When the cutting edge of the tool approaches an element in the cutting zone, the plastic strain of the element in the work piece increases and reaches the failure strain even before the tool completely crosses over the length of that element leading to

the deletion. This causes the force values to drop down at that instant but only for a very little time in which the tool reaches the next successive element. The frequency of occurrence of the above stated process is so high leading to a force output with high noise/vibration.

- The tool was modeled as a rigid body in the current model and does not have any impact due to the cutting process. But in actual case, the tool is deformable, and is subjected to wear. It is really hard to model such a simulation incorporating the effects of tool as it would increase the computation time.

- The advantage of the material model used in this study is that it helps in modeling the kinematic hardening effect which is really exhibited by Aluminum 6061 T6 alloy [23]. The limitation being, it does not account for the thermal effects which influence the force values to an extent. Also the failure plastic strain is given in the input by the user which is not the case with other material models like Johnson-Cook were it calculates the failure strain rates based a set of coefficients.

- Another limitation that was observed in this simulation was element deletion in the secondary deformation zone and along the line of cut. This deletion takes place based on the failure plastic strain of the elements which if not deleted becomes highly distorted and lead to numerical instability causing the simulation to stop. This was also limiting factor for cut chip thickness measurement, as the chip thickness of the cut chip showed that it increased in thickness by a small amount but not the same as predicted by the experiments. The plot in figure 33 shows that the simulated ratio of chip thickness was always greater than the

experimental thickness ratio but the simulated results showed that the ratio increased with increase in uncut chip thickness at constant rake angle following the trend shown by experimental results. Since this measurement is only a rough estimate the variation is only shown for one of the cases, while other options of predicting the ratio to higher accuracy would be explored in the future work.

- Friction modeling adapted in the current study is a static friction model to reduce computational time which is not the case with real time experiments. Moreover, the friction values used were calculated from the experimental results based on the Merchant's metal cutting equations which had a very high range from 0.2855 to 1.029.

- The current simulation model takes about 30 hours in an average on a single processor super computer to reach a stable state which is one of the disadvantages of using such finite element methods.

- It is hard to find a material model that exactly describes the behavior of the work material as it is very hard to built one that addresses all the aspects. For example, the kinematic plastic model helps to describe well the kinematic hardening nature of Al6061 –T6 alloy but fails to account for thermal effects. In case of Johnson-Cook, it addresses the hardening nature and as well the thermal effects, nut the hardening type used in not kinematic hardening.

A recap of the force value comparisons:

- Villumsen, Morten, F., and Fauerholdt, Torben, G., used [15] Ls Dyna to simulate an orthogonal machining of Al 6082 and the results obtained were; F (thrust) was under estimated by 60% and F (cutting) was over estimated upto 104%.

- Komvopoulus and Erpenbeck [6] generated force values from simulation, that were off by upto 160 N on Fp and upto 130 N on Fn.

- Zhang and Bagchi [7] in their experiments obtained the feed force and the cutting force to be in good agreement with the experimental results, but were using very high velocity values of upto 238 mm/s.

- Huang and Black [9] in their work reported that the cutting force obtained from the model was 969 N whereas the experimental values were 1060 N.

- The force values obtained by Schermann, T., Marsolek, J., Schmidt, C., and Fleischer, J., [77] was found to be in close agreement with the experimental values, but a constant friction coefficient value was used even when the rake angle changed.

- Arrazola, P, J., Ugarte, D., Montoya, J., Villar, A., and Marya, S., [11] predicted the cutting forces in an orthogonal machining of AISI 4140 steel to be 126N using ABAQUS and 216 N using AdvantEdge whereas the experimental result showed that it was 189N.

- Svoboda, Ales., Wedberg, Dan., and Lindgren, Lars-Erik., [76] utilized two different material models to orthogonal metal cutting process in MSC.Marc finite element software and the force values obtained by him were varying upto 19.9%. for cutting force and upto 8.9% for thrust force.

- Espinaso et.al., [78] used Smoothed particle hydrodynamic method to predict the cutting forces for a orthogonal machining of Al 6061 T6 alloy and reported that the cutting force variation was upto 10% and the thrust force upto 30%.

- Some variation to the current model like altering the element shapes were tried, where a triangular shell element was used in place of a 4 node shell element, it made the model too stiff and resulted in errors and killing the simulation as soon as it began to run.

- A Johnson Cook material model was tried for one case to see if really had an impact on the output, and found that the simulation was terminated by half way due to high element distortion. A very fine mesh with approximately 60,000 nodes was also tried and resulted in termination again due to highly distorted elements. This leads us to rethink the meshing control adopted in the present model and the need to utilize some advanced techniques like adaptive remeshing or meshless techniques like Smoothed Particle Hydrodynamics (SPH) for future work.

Conclusions

Based on the analysis of the simulation results following conclusions are made on the simulation model, cutting forces and thrust forces obtained from the simulations.

- The simulation model underestimates both the force values (thrust and cutting). The cutting force variation is within 20% of the experimental results whereas the thrust force is one third of the experimental results. And the variation of thrust force by a factor of three is almost applicable to all the combinations considered in the present study.

- The simulated cutting forces increase with increase in uncut chip thickness at constant rake tool angle. The thrust forces form the simulation increase when the uncut chip thickness changes from 0.001” to 0.005” at constant tool rake angle.

- A decrease in cutting force is observed when the tool rake angle increases from a -10° to 30° for all uncut chip thickness.

- The simulated thrust force is found to be decreasing with increase in tool rake angle for all uncut chip thickness. The decrease is not as high as observed in experimental results. In all the above cases, the trends in variation of the simulated data are similar to the trends in variation of the experimental data but not in magnitude.

Scope for Future Work

The current simulation model is just a basic set up to demonstrate the capability of LS Dyna to model metal cutting problems. This model can be fine tuned, so that the forces predicted by the model will strongly validate the experimental results. Various things that could be added on to the current setup which were not tried in this study due to lack time are:

- Different or new material models can be used to best describe the behavior of the work piece and tool material. A sensitivity analysis could be performed by varying the variable parameter and determine how well the model is responds to the changes

- Implement an alternative method that would address the tool –work piece friction similar to the actual experiment. A friction coefficient range for a particular material combination of interest could be determined from tribological experiments or literature.

- New techniques like Adaptive Lagrangian Eulerian method along with adaptive remeshing could be used to avoid element distortion, but will take more computational time. A mesh free finite element analysis technique like Smoothed Particle Hydrodynamics (SPH) could be used.

References

1. Merchant, M.E., "Mechanics of the Metal Cutting Process," *Journal of Applied Physics*, Vol. 16, pp 267 -275, 1945.
2. Komanduri, R., Raff, L.M., "A review of the molecular dynamics simulation of machining at the atomic scale", *Proc. Instn. Mech. Engrs.* , Vol. 215 Part B, pp 1639 -1672, 2001.
3. Payton, Lewis, N., "A Basic Correction to the Orthogonal Metal Cutting Models", *Proceedings of the ASME 2009 International Manufacturing Science and Engineering Conference*, MSEC2009.
4. Carroll, John, T (III)., and Strenkowski, John, S., "Finite Element Models of Orthogonal Cutting with Application of Single Point Diamond Turning", *Int. J. Mech Sci*, Vol 30, No 12, pp 899 -920, 1988.
5. Shih, Albert, J, M., Chandrasekar, S., and Yang, Henry, T, Y., "Finite element Simulation of Metal Cutting Process with Strain- Rate and Temperature Effects", *Fundamental Issues in Machining*, ASEM PED –Vol 43, pp 11, 1990.
6. Komvopoulos, K., and Erpenbeck, S, A., "Finite Element Modeling of Orthogonal Metal Cutting", Journal *of Engineering for Industry*, Vol, 113 pp 253 – 267, 1991.

7. Zhang, Bingqi., and Bagchi, Amit., “Finite Element Simulation of Chip Formation and Comparison with Machining Experiment”, Computational Methods in Materials Processing, MD- Vol. 39/PED Vol. 61, ASME 1992.
8. Marusich, T, D., and Ortiz, M., “A Parametric Finite Element Study of Orthogonal High-Speed Machining”, *Internat. J. Num. Methods Engrg.* , 1995.
9. Haung, J, M., and Black, J.T., “An Evaluation of Chip Formation Criteria for the FEM Simulation of Machining”, *Journal of Manufacturing Science and Engineering*, Vol. 118, pp 545-554, 1996.
10. Marusich, Troy, D., “Effects of Friction and Cutting Speed on Cutting Force”, *Proceedings of ASME Congress*, 2001.
11. Arrazola, P, J., Ugarte, D., Montoya, J., Villar, A., and Marya, S., “Finite Element Modeling of Chip Formation Process with ABAQUS/EPLICIT 6.3”, *VIII International Conference on Computational Plasticity*, 2005.
12. Pramanik, A., Zhang, L, C., and Arsecularatne, J, A., “An FEM investigation into the behavior of metal matrix composites: Tool-particle interaction during orthogonal cutting”, *International Journal of Machine Tools and Manufacture 47*, pp 1497-1506, 2007.
13. Masillamani, David, P., and Chessa, Jack., “Determination of Optimal Cutting Conditions in Orthogonal metal Cutting Using LS-DYNA with Design of Experiments Approach”, 8th International LS-DYNA Users Conference, May 2004, Dearborn, MI, USA.

14. Raczy, A., Altenhof, W,J., and Alps, A, T., “An Eulerian Finite Element Model of the Metal Cutting Process”, 8th International LS-DYNA Users Conference, May 2004, Dearborn, MI, USA.
15. Villumsen, Morten, F., and Fauerholdt, Torben, G., “Prediction of Cutting Forces in Metal Cutting, Using the Finite Element Method, a Lagrangian Approach”, LS-DYNA Anwenderforum, Bamberg, 2008.
16. Su, Chong., Hou, Jun-Ming., Zhu, Li-da., and Wang, Wan-shan., “Finite Element Analysis of Two Dimensional metal Cutting process”, The 3rd International Conference in innovative Computing Information and Control. IEEE 2008.
17. Yuming, Zhu., and Guicheng, Wang., “Simulation Model and Mechanism of Burr Formation”, International Workshop on Modeling, Simulation and Optimization, IEEE 2008.
18. Oxley, P.L.B., 1989, Mechanics of Machining, An Analytical Approach to Assessing Machinability. Halsted Press, John Wiley & Sons Limited, New York.
19. Zerilli, F, J., and Armstrong, R, W., “Dislocation mechanics based constitutive relations for material dynamics calculations”, *Journals of Applied Physics*, Vol. 61/5, pp 1816-1825, 1987.
20. Johnson G, R., and Cook, W, H., “A constitutive model and data for metals subjected to large strains, high strain rates and high temperatures”, Proceedings of the 7th International Symposium on Ballistics, The Hauge, The Netherlands, pp 541- 547, 1983.

21. Lesuer, D, R., kay, G, J., and LeBlanc, M, M., “Modeling large –Strain, high-Rate Deformation in Metals”, Third Biennial Tri-Laboratory Engineering Conference Modelling and Simulation, CA USA, 1999.
22. Altenhof, W., and Ames, W., “Strain rate effects for Aluminum and Magnesium alloy in Finite element Simulations of steering wheel armature impact test”, *Fatigue Fract. Engng. Mater. Struct 25*, pp 1149-1156, 2002.
23. Khan, Akthar, S., Pandey, Amit., and Stoughton, Thomas., “Evolution of subsequent yield surfaces and elastic constants with finite plastic deformation. Part III: Yield surface in tension –tension stress space (AL 6061-T6511 and annealed 110 Al)”, *International Journal of Plasticity 26*, pp 1432 – 1411, 2010.
24. Cocquilhat, M. (1851). Annales des Travaus Publics en Belgigque 10: 199
25. Joessel, H. (1865). Annuaire de la Societe des Anciens Eleves des Ecoles Imperiales D'Arts et Meteiers.
26. Time, I. (1877). Memoire sur le Rabotage de Metaux. St. Petersburg, Russia.
27. Tresca, H. (1878). Proceedings of the Institution of Mechanical Engineers: 301.
28. Mallock, A. (1881). Proceedings of the Royal Society of London 33: 127.
29. Haussner, A. (1892). Das Holben von Metallen. Wien: 117.
30. Zvorkin, N. N. (1893). Rabota I Usilie Neobkhodimyya dlya Oteleniya Metallicheskikh Struzhek. Moscow, Russia.
31. “Ingenieur and Maschininenmechanick” handbook (1896), Berlin, IG.
32. Lindner, G. (1907). Zeitschrift VDI 51: 1070.
33. Ernst, H. and M. E. Merchant (1941). Chip Formation, Friction and Finish. Cincinnati, Ohio, The Cincinnati Milling Machine Company.

34. Piispanen, V. (1937). Teknillinen Aikakauslehti 27: 315

35. Merchant, M. E. (1945). *Journal of Applied Physics* 16: 267.

36. Coker, E. and K. Chakko (1925). Proceedings of the Institution of Mechanical Engineers: 357.

37. Coker, E. (1922). Proceedings of the Institution of Mechanical Engineers: 567.

38. Ishi, S. (1929). Macroscopic Kinematographs Applied to Research in Metal Cutting. World Engineering Conference, Tokyo, Japan.

39. Schwerd, F. (1935). Zeitschrift VID 80: 233.

40. Boston, O. W. (1930). Transactions of ASME 52: 119.

41. Herbert, E. G. (1926). Transactions of ASME 48: 705.

42. Boothroyd, G., W. A. Knight and NetLibrary Inc. (1989). Fundamentals of Machining and Machine tools. New York, Marcel Dekker.

43. Eggleston, D. M., R. Herzog and E. G. Thomsen (1959). *Journal of Engineering for Industry*: 263.

44. Lee, E. H. and B. W. Shaffer (1951). *Journal of Applied Mechanics 18(*4): 405.

45. Okushima, K. and K. Hitomi (1961). *ASME Journal of Engineering for Industry*: 545.

46. Zorev, N. N. (1966). Metal Cutting Mechanics. Oxford, New York,, Pergamon Press.

47. Von Luttervelt, C. A. (1977). Annals of the CIRP 25(1): 33.

48. Black, J T. (1979). *ASME Journal of Engineering for Industry* 101: 403.

49. Black, J T. and N.D. Briggs (1994) *Tribology Symposium, ASME,* PD Vol. 61, p. 41.

50. Huang, J. M. (1996). PhD Dissertation, Auburn, AL, Auburn University.

51. Komanduri, R. and R. H. Brown (1981). *Journal of Engineering for Industry* 103: 33.

52. Komanduri, R. and R. H. Brown (1982). *Journal of Engineering for Industry* 103: 33.

53. Lemaire, J. C. and W. A. Backofen (1972). Metallurgical Transactions 3: 477

54. Sullivan, K. F., P. K. Wright and P. D. Smith (1978). Metals Technology: 181.

55. Shaw, M. C. (1993). Annals of the CIRP 42(1): 29.

56. Cook, N. H., L. Finnie and M. C. Shaw (1954). ASME Transactions 76: 153.

57. Loewen, E. G. and M. C. Shaw (1954). Transactions of ASME: 217.

58. Komanduri, R. and T. Schroeder (1986). *Journal of Engineering for Industry* 108: 93

59. Komanduri, R., K. Subramanian, B. F. v. Turkovich, American Society of Mechanical Engineers. Production Engineering Division. and American Society of Mechanical Engineers. Winter Meeting (1984). High speed machining : presented at the Winter Annual Meeting of the American Society of Mechanical Engineers, New Orleans, Louisiana, December 9-14, 1984. New York, N.Y., American Society of Mechanical Engineers.

60. Ling, F. F. and M. B. Peterson (1987). Approaches to Modeling Friction and Wear. F. F. Ling and C. T. H. Pan, Springer-Verlag.

61. Kopalinsky, E. M., X. Li and P. L. B. Oxley (1991). Tribological Aspects in Manufacturing, ASME.

62. Thomsen, E. G. (1969). Annals of the CIRP 17: 187.

63. Hitomi, K. and G.L. Thuering (1962). *Journal of Engineering for Industry*, May: 282.

64. Ham, I., K. Hitomi and G. L. Thuering (1961). Transactions of ASME B83: 282.

65. Zouhar, J., and Piska, M., "Modelling the Orthogonal Machining Process using Cutting Tools with Different Geometry", Faculty of Mechanical Engineering, Brno UT, Czech Republic.

66. Ozel, Tugrul., and Karpat, Yigit., " Identification of Constitutive Material model parameters for high strain rate metal cutting conditions using evolutionary computational algorithims", *Materials and Manufacturing processes 22,* pp 659-667, 2007.
67. Payton, L.N., "Orthogonal Machining of Copper using a Virtual Quick stop Device", Master's Thesis, Auburn University, USA, June 2000.
68. Song, X., "Experimental studies and Numerical Simulations of Continuous and Discontinuous Chip Formation during Orthogonal Cutting", Master's Thesis, University of Windsor, Canada, 2005.
69. Maftah, Abdulfatah., "Finite Element Simulation of orthogonal metal Cutting using an ALE Approach", Master's Thesis, University of New Brunswick, Canada, April 2008.
70. Araujo, C, M., "Non-Linear Kinematic Hardening model for Multiaxial Cyclic Plasticity", Master's thesis, Louisiana State University, USA, August 2002.
71. Sripathi, P.S., "Investigation into the effects of Tool Geometry and Metal Working Fluids on Tool Forces and Tool Wear during Orthogonal Tube Turning of Aluminum 6061 Alloy", Master's Thesis, Auburn University, USA, December 2009.
72. "Abaqus user manual", Dassault Systemes Simulia Corp, RI, USA.
73. "LS-DYNA Theory Manual", Livermore Software Technology Corporation, CA, USA, LSTC.com, March 2006, http://www.lstc.com/pdf/ls-dyna_theory_manual_2006.pdf (accessed March 2, 2011).
74. ASM International., "ASM hand book, Metals Process Simulation", Vol. 22B; Furrer, D, U., and Semiantin, S, L., *Eds*; ASM International: USA, 2010; pp 361-371.

75. http://www.matweb.com/search/DataSheet.aspx?MatGUID=1b8c06d0ca7c456694c7777d9e10be5b&ckck=1 (accessed May 20, 2011.)
76. Svoboda, Ales., Wedberg, Dan., and Lindgren, Lars-Erik., "Simulation of metal cutting using physically based plasticity models", Modeling and Simulation in Materials Science and Engineering, 18, IOP Publishing, 2010.
77. Schermann, T., Marsolek, J., Schmidt, C., and Fleischer, J., "Aspects of the Simulation of a cutting process with ABAQUS/Explicit including the interaction between the cutting process and the dynamic behavior of the machine tool", University of Karlsruhe, Institute of Production Science, Germany.
78. Espinosa, C., Lacome, J, L., Limido, J., Salaun, M., Mabru, C., and Chieragatti, R., "Modelling High Speed Machining with SPH method", 10th International LS-DYNA Users Conference, Dearborn, MI USA, June 2008.
79. Degarmo, Paul, E., Black J T., Kohser, Ronald, A., Fundamentals of Machining/ Orthogonal Machining. "*Materials and Processing in Manufacturing*" Ninth Edition; John Wiley & sons, Inc: USA, 2003; pp 497, 498 and 492.
80. Black, J, T., and Huang, J, M., "Shear Strain model in Metal Cutting", Manufacturing Science and Engineering, MED – Vol. 2-1 / MH –Vol. 3-1; ASME 1995, pp 283- 302.
81. Klamecki, B, E., and Kim, S., "On the Plane stress to Plane strain Transition Across the Shear Zone in Metal Cutting", Transactions of the ASME, Vol. 110, November 1988, pp.322-325.

Appendix 1: Material Properties

Material property used in modeling Work piece Aluminum 6061 –T6 Alloy [21, 75]

S.no	Material property	Value	Units
1	Density	2700	Kg/m3
2	Young's modulus	68.9	GPa
3	Poisons ratio	0.33	-
4	Yield strength (tensile)	276	MPa
5	Cowper Symonds Coefficient (C)	6000	-
6	Cowper Symonds Coefficient (P)	4	-
7	Failure Plastic strain	1.15	-

Material property used in modeling Tool, Steel [75]

S.no	Material property	Value	Units
1	Density	3200	Kg/m3
2	Young's Modulus	300	GPa
3	Poison's ratio	0.28	-

Appendix 2: Force Values from Simulation

Table Below gives the cutting force and thrust force values of both experiment and simulation for all combinations of tool rake angle and depth cuts.

Run No.	Rake Angle (α)	DOC (inches)	EXP Fc (N)	Simulation Fc (N)	EXP Ft (N)	Simulation Ft (N)
1	-10	0.001	180.0885	104.61	184.6579	31.7
2	-10	0.002	269.8323	190.2	259.0394	79.25
3	-10	0.003	339.9456	285.3	311.4947	120.46
4	-10	0.004	413.5737	380.4	363.4291	142.65
5	-10	0.005	476.4275	475.5	410.9382	158.5
6	0	0.001	172.0512	95.1	174.9053	31.7
7	0	0.002	256.0913	158.5	221.5214	63.4
8	0	0.003	326.2599	253.6	296.1015	95.1
9	0	0.004	405.6773	317	367.3833	126.8
10	0	0.005	455.4033	412.1	325.5767	104.61
11	15	0.001	121.1535	79.25	65.2636	31.7
12	15	0.002	201.5158	158.5	114.1896	34.925
13	15	0.003	263.9330	221.9	145.5129	41.21
14	15	0.004	349.1896	285.3	204.4720	47.55
15	15	0.005	409.3102	332.85	224.7502	63.4
16	30	0.001	116.7896	88.76	63.6969	22.19
17	30	0.002	181.4515	126.8	86.5498	25.36
18	30	0.003	239.1273	158.5	97.7236	31.7
19	30	0.004	318.7960	221.9	140.6939	47.55
20	30	0.005	337.29396	253.6	95.308572	63.4

Appendix 3: LS Dyna Input file sample

```
$# LS-DYNA Keyword file created by LS-PrePost 3.1 -
02Apr2011(09:25)
$# Created on Jun-26-2011 (21:18:16)
*KEYWORD
*TITLE
$# title

*CONTROL_CONTACT
$#  slsfac    rwpnal    islchk    shlthk    penopt    thkchg
orien    enmass
  1.000000                 1
1
$#  usrstr    usrfrc     nsbcs    interm     xpene     ssthk
ecdt   tiedprj
                                        4.000000
$#   sfric     dfric       edc       vfc        th     th_sf
pen_sf

$#  ignore    frceng   skiprwg    outseg   spotstp   spotdel
spothin

$#    isym    nserod    rwgaps    rwgdth     rwksf      icov
swradf    ithoff
                                        1.000000
$#  shledg


*CONTROL_ENERGY
$#    hgen      rwen    slnten     rylen
         2         2         2         2

*CONTROL_SHELL
$#  wrpang     esort     irnxx    istupd    theory       bwc
miter      proj
 20.000000         1        -1         1         2         2
1
$# rotascl    intgrd    lamsht    cstyp6    tshell    nfail1
nfail4   psnfail
```

```
  1.000000                              1                   1
1
$# psstupd    irquad     cntco

*CONTROL_TERMINATION
$#  endtim    endcyc     dtmin    endeng    endmas
 5.0000E-4

*CONTROL_TIMESTEP
$#  dtinit    tssfac      isdo    tslimt     dt2ms      lctm
erode     ms1st
            0.900000
$#  dt2msf   dt2mslc     imscl

*DATABASE_MATSUM
$#      dt    binary      lcur     ioopt
 5.0000E-7                              1

*DATABASE_NODFOR
$#      dt    binary      lcur     ioopt
 1.0000E-7                              1

*DATABASE_BINARY_D3PLOT
$#      dt      lcdt      beam     npltc    psetid
 1.0000E-6
$#   ioopt

*DATABASE_BINARY_D3THDT
$#      dt      lcdt      beam     npltc    psetid
 5.0000E-7

*DATABASE_FORMAT
$#   iform   ibinary

*DATABASE_EXTENT_BINARY
$#   neiph     neips    maxint    strflg    sigflg    epsflg
rltflg    engflg
                                3         1         0         0
0         0
$#  cmpflg    ieverp    beamip     dcomp      shge     stssz
n3thdt   ialemat
                                4         0         0         0
0         0
$# nintsld   pkp_sen      sclp    unused     msscl     therm
intout    nodout
                          1.000000
STRESS    STRESS

*DATABASE_NODAL_FORCE_GROUP
$#    nsid       cid
```

```
         7

*DATABASE_HISTORY_NODE
$#     id1       id2       id3       id4       id5       id6
id7       id8
         1

*BOUNDARY_PRESCRIBED_MOTION_SET
$#    nsid       dof       vad      lcid        sf       vid
death     birth
         1         1         2         1  1.000000
0.000

*BOUNDARY_PRESCRIBED_MOTION_SET
$#    nsid       dof       vad      lcid        sf       vid
death     birth
         2         2         2         2  1.000000
0.000

*BOUNDARY_PRESCRIBED_MOTION_SET
$#    nsid       dof       vad      lcid        sf       vid
death     birth
         3         7         2         3  1.000000
0.000

*BOUNDARY_PRESCRIBED_MOTION_SET
$#    nsid       dof       vad      lcid        sf       vid
death     birth
         4         1         2         4  1.000000
0.000

*BOUNDARY_PRESCRIBED_MOTION_SET
$#    nsid       dof       vad      lcid        sf       vid
death     birth
         5         2         2         5  1.000000
0.000

*BOUNDARY_PRESCRIBED_MOTION_SET
$#    nsid       dof       vad      lcid        sf       vid
death     birth
         6         7         2         6  1.000000
0.000

*BOUNDARY_PRESCRIBED_MOTION_RIGID
$#     pid       dof       vad      lcid        sf       vid
death     birth
         2         1         2         7  1.000000
0.000

*CONTACT_2D_AUTOMATIC_SINGLE_SURFACE_ID
```

```
$#     cid
title
         1
$#    sids      sidm     sfact      freq        fs        fd
dc     membs
         3            1.000000        50  0.300000  0.300000
6
$#  tbirth    tdeath       sos       som       nds       ndm
cof      init
          1.0000E+20     0.000     0.000

*SET_PART_LIST
$#     sid       da1       da2       da3       da4    solver
         3
$#    pid1      pid2      pid3      pid4      pid5      pid6
pid7      pid8
         1         2

*PART
$# title
Part          1 for Mat         1 and Elem Type         1
$#     pid     secid       mid     eosid      hgid      grav
adpopt      tmid
         1         1         1

*SECTION_SHELL
$#   secid    elform      shrf       nip     propt   qr/irid
icomp     setyp
         1        13  1.000000         4         1
3
$#      t1        t2        t3        t4      nloc     marea
idof    edgset


*MAT_PLASTIC_KINEMATIC
$#     mid        ro         e        pr      sigy      etan
beta
         1 2700.00006.8900E+10  0.330000 2.7000E+8
$#     src       srp        fs        vp
 6000.0000  4.000000  1.150000  1.000000

*PART
$# title
Part          2 for Mat         2 and Elem Type         1
$#     pid     secid       mid     eosid      hgid      grav
adpopt      tmid
         2         1         2

*MAT_RIGID
```

```
$#     mid        ro          e         pr          n    couple
m     alias
         2 3200.0003.0000E+11  0.280000
$#     cmo      con1      con2
  1.000000         7         7
$# lco or a1      a2        a3        v1        v2        v3


*DEFINE_CURVE
$#    lcid      sidr       sfa       sfo      offa      offo
dattyp
         1            1.000000  1.000000
$#                a1                  o1

      5.0000002e-004

*DEFINE_CURVE
$#    lcid      sidr       sfa       sfo      offa      offo
dattyp
         2            1.000000  1.000000
$#                a1                  o1

      5.0000002e-004

*DEFINE_CURVE
$#    lcid      sidr       sfa       sfo      offa      offo
dattyp
         3            1.000000  1.000000
$#                a1                  o1

      5.0000002e-004

*DEFINE_CURVE
$#    lcid      sidr       sfa       sfo      offa      offo
dattyp
         4            1.000000  1.000000
$#                a1                  o1

      5.0000002e-004

*DEFINE_CURVE
$#    lcid      sidr       sfa       sfo      offa      offo
dattyp
         5            1.000000  1.000000
$#                a1                  o1

      5.0000002e-004

*DEFINE_CURVE
```

```
$#    lcid      sidr       sfa       sfo      offa      offo
dattyp
         6         1.000000  1.000000
$#                a1                  o1

      5.0000002e-004


*DEFINE_CURVE
$#    lcid      sidr       sfa       sfo      offa      offo
dattyp
         7         1.000000  1.000000
$#                a1                  o1

      5.0000002e-004          -0.0010500

*SET_NODE_LIST
$#     sid       da1       da2       da3       da4    solver
         1
$#    nid1      nid2      nid3      nid4      nid5      nid6
nid7      nid8
      2212      2232      2233      2234      2235      2236
2237      2238
      2239      2240      2241      2242      2243      2244
2245      2246
      2247      2248      2249      2250      2251      2252
2253      2254
      2255      2256      2257      2258      2259      2260
2261      2262
      2263      2264      2265      2266      2267      2268
2269      2270
Contd.

*SET_NODE_LIST
$#     sid       da1       da2       da3       da4    solver
         2
$#    nid1      nid2      nid3      nid4      nid5      nid6
nid7      nid8
      2212      2232      2233      2234      2235      2236
2237      2238
      2239      2240      2241      2242      2243      2244
2245      2246
      2247      2248      2249      2250      2251      2252
2253      2254
      2255      2256      2257      2258      2259      2260
Contd.

*SET_NODE_LIST
$#     sid       da1       da2       da3       da4    solver
```

```
         3
$#     nid1       nid2       nid3       nid4       nid5       nid6
nid7       nid8
       2212       2232       2233       2234       2235       2236
2237       2238
       2239       2240       2241       2242       2243       2244
2245       2246
```
Contd.

```
*SET_NODE_LIST
$#      sid        da1        da2        da3        da4     solver
         4
$#     nid1       nid2       nid3       nid4       nid5       nid6
nid7       nid8
        12        212        213        214        215        216
217        218
       219        220        221       2232       2432       2433
2434       2435
       2436       2437       2438       2439       2440       2441
2442       2443
       2444       2445       2446       2447       2448       2449
2450

*SET_NODE_LIST
$#      sid        da1        da2        da3        da4     solver
         5
$#     nid1       nid2       nid3       nid4       nid5       nid6
nid7       nid8
        12        212        213        214        215        216
217        218
       219        220        221       2232       2432       2433
2434       2435
       2436       2437       2438       2439       2440       2441
2442       2443
       2444       2445       2446       2447       2448       2449
2450

*SET_NODE_LIST
$#      sid        da1        da2        da3        da4     solver
         6
$#     nid1       nid2       nid3       nid4       nid5       nid6
nid7       nid8
        12        212        213        214        215        216
217        218
       219        220        221       2232       2432       2433
2434       2435
       2436       2437       2438       2439       2440       2441
2442       2443
```

```
      2444      2445      2446      2447      2448      2449
2450

*SET_NODE_LIST
$#     sid       da1       da2       da3       da4    solver
         7                                        MECH
$#    nid1      nid2      nid3      nid4      nid5      nid6
nid7      nid8
      2212      2232      2233      2234      2235      2236
2237      2238
      2239      2240      2241      2242      2243      2244
2245      2246
      Contd.

*ELEMENT_SHELL
$#   eid     pid      n1      n2      n3      n4      n5      n6
n7      n8
       1       1       1     420     421       3
       2       1     420     419     430     421
       3       1     419     418     439     430
       4       1     418     417     448     439
       5       1     417     416     457     448
       6       1     416     415     466     457
       7       1     415     414     475     466
      ...
      ...
      ...
    6087       2    6318    6273    6272    6324
    6088       2    6323    6274    6273    6318
    6089       2    6322    6275    6274    6323
    6090       2    6319    6276    6275    6322
    6091       2    6321    6277    6276    6319

*NODE
$#   nid               x               y               z      tc
rc
       1       0.0020000  4.8749999e-004
       2       0.0020000  3.6050001e-004
       3       0.0020000  4.4214245e-004
       4       0.0020000  4.1277439e-004
       5       0.0020000  3.9375920e-004
       6       0.0020000  3.8144726e-004
       7       0.0020000  3.7347554e-004
       8       0.0020000  3.6831404e-004
       9       0.0020000  3.6497205e-004
      10       0.0020000  3.6280820e-004
      11       0.0020000  3.6140715e-004
      ...
       ...
       ...
```

```
    6346       0.0021769  4.6832458e-004
    6347       0.0021032  4.2985147e-004
    6348       0.0022402  5.4376246e-004
*END
```